nature communications

Article

https://doi.org/10.1038/s41467-024-53430-y

Enhancing glymphatic fluid transport by pan-adrenergic inhibition suppresses epileptogenesis in male mice

Received: 14 January 2023

Accepted: 8 October 2024

Published online: 06 November 2024

Check for updates

Qian Sun[1,2,5], Sisi Peng[1,3,5], Qiwu Xu[1], Pia Weikop[4], Rashad Hussain[1], Wei Song[1], Maiken Nedergaard[1,4] ✉ & Fengfei Ding[1,2] ✉

Epileptogenesis is the process whereby the previously normally functioning brain begins to generate spontaneous, unprovoked seizures. Status epilepticus (SE), which entails a massive release of neuronal glutamate and other neuroactive substances, is one of the best-known triggers of epileptogenesis. We here asked whether pharmacologically promoting glymphatic clearance during or after SE is beneficial and able to attenuate the subsequent epileptogenesis. We induced SE in adult male mice by intrahippocampal kainic acid (KA) infusion. Acute administration of a cocktail of adrenergic receptor antagonists (propranolol, prazosin, and atipamezole: PPA), enhanced glymphatic flow and effectively reduced the severity of spontaneous seizures in the chronic phase. The PPA treatment also reduced reactive gliosis and inhibited the loss of polarized expression of AQP4 water channels in the vascular endfeet of astrocytes. Administration of PPA after cessation of SE (30 hours post KA) also effectively suppressed epileptogenesis and improved outcome. Conversely, mice with constitutively low glymphatic transport due to genetic deletion of the aquaporin 4 (AQP4) water channel showed exacerbation of KA-induced epileptogenesis. We conclude that the pharmacological modulation of glymphatic fluid transport may represent a potential strategy to dampen epileptogenesis and the occurrence of spontaneous seizures following KA-induced SE.

Epilepsy is a neurological disorder that is often associated with cognitive and psychological disturbances arising from recurrent epileptiform discharges that can be refractory to medical treatment[1]. Acquired epilepsy can follow in the aftermath of several types of brain insults, such as status epilepticus (SE) or traumatic injury. There is characteristically a delay lasting from months to years after the initial insult to the first unprovoked seizure heralding chronic epilepsy[2,3], thus implying an incubation period, while providing a broad window for therapeutic interventions. The severity of the initial SE is directly linked with the long-term outcomes[4], although the precise mechanisms of epileptogenesis are poorly understood. In the past three decades, there have been more than ten randomized clinical trials aiming at tackling post-traumatic epileptogenesis, including the trials with phenobarbital, phenytoin, carbamazepine, and valproic acid[5,6], none of which have yet proved to be effective[7,8]. There is clearly a need for new strategies to prevent epileptogenesis as a sequela of SE.

[1]Center for Translational Neuromedicine, University of Rochester, Rochester, NY, USA. [2]Department of Pharmacology, School of Basic Medical Sciences, State Key Laboratory of Medical Neurobiology and Ministry of Education Frontiers Center for Brain Science, Institutes of Brain Science, Shanghai Medical College, Fudan University, Shanghai, China. [3]Department of PET/MR, Shanghai Universal Medical Imaging Diagnostic Center, Shanghai, China. [4]Center for Translational Neuromedicine, University of Copenhagen Faculty of Health and Medical Sciences, Copenhagen, Denmark. [5]These authors contributed equally: Qian Sun, Sisi Peng. ✉e-mail: nedergaard@urmc.rochester.edu; Fengfei_ding@fudan.edu.cn

Excessive excitatory activity drives synaptic potentiation of the entorhinal cortex in the initial stages of SE[9]. Several lines of evidence document modification of hippocampal microcircuit activity[10,11], and the reorganization of neuronal networks via excitatory axonal sprouting after a SE event[12–14]. The microenvironment changes, which include factors such as neurotransmitters, inorganic ions, cytokines, and the extracellular volume, could all contribute to the neuronal network re-organization post SE[15–25]. Recent studies highlight the role of glymphatic transport in brain fluid and solute clearance[26,27]. Glymphatic flow is a highly organized system for fluid transport system along the perivascular space surrounding the cerebral vasculature. Astrocytic vascular endfeet plastering the vascular wall create the perivascular space for glymphatic flow, and the polarized expression of aquaporin 4 (AQP4) on the astrocytic endfeet imparts important mediation of fluid influx. Genetic deletion or pharmacological inhibition of AQP4 reduces glymphatic fluid influx and efflux, which consequently inhibits the clearance of extracellular substances from the brain[28–30]. The state of glymphatic function is strongly regulated across the sleep/wake cycle[31,32], being most active during sleep, when norepinephrine (NE) tone is low due to the physiological silencing of the locus coeruleus. Indeed pharmacological antagonism of receptors for the arousal-promoting neurotransmitter NE enhances glymphatic transport[32]. Furthermore, pan-adrenergic receptor inhibition via administering a cocktail of α1, α2, and β receptor blockers accelerates glymphatic fluid transport and improves outcomes in models of acute stroke or traumatic brain injury[33–35]. Because SE is associated with a massive release of neuronal glutamate and other neuroactive compounds, which might influence glymphatic clearance, we predicted that pharmacological manipulation of glymphatic clearance might moderate the severity of acquired epilepsy.

To test this hypothesis, we used a murine model with an intrahippocampal infusion of the excitatory substance kainic acid (KA) to trigger SE, setting the stage for a chronic seizure disorder. After a latent period, KA-infused mice develop spontaneous epileptic discharges that share several features with temporal lobe epilepsy[36–38]. We tested whether pan-inhibition of adrenergic receptors upon initiation or after cessation of SE could improve long-term outcomes, using seizure rate as our endpoint. Conversely, we used a group of AQP4 knockout mice to assess whether chronic suppression of glymphatic flow would potentiate epileptic discharges in chronic phase. The observations supported the notion that glymphatic transport is a potent moderator of the severity of epilepsy arising after SE.

Results

Characterization of status epilepticus induced by intrahippocampal kainic acid infusion

Mesial temporal lobe epilepsy is a major contributor to medically refractory epilepsies and is the most frequent type of epilepsy referred to surgical centers[39]. Mesial temporal lobe epilepsy can arise spontaneously, or can be acquired in the setting of brain injury involving tumors, infection, stroke, childhood high fever, traumatic brain injury, or status epilepticus[40,41]. Unilateral intrahippocampal infusion of kainic acid (KA) is a widely used rodent model of mesial temporal lobe epilepsy. An intrahippocampal KA infusion provokes an acute phase of continuous epileptiform activity, followed by development of spontaneous seizures after a latent period[36,42]. Thus, the KA model provides a time window for studying the process of epileptogenesis. The severity of acute onsets determines the frequency of the spontaneous seizures and the extent of brain pathology in the chronic phase[43]. We here recorded behavioral and EEG/EMG signals for three days after intrahippocampal KA infusion (Fig. 1A). We defined a period of featured active epileptiform activity, termed as “established SE”, which is composed with two distinct phases. The onset of the first convulsive seizure in phase 1 occurred at 0.9 ± 0.3 h post KA infusion. In total, we recorded 11.8 ± 2.2 convulsive seizures with mean Racine scale 4.5 ± 0.3 over a period of 4.8 ± 1.5 hours in phase 1 (Fig. 1F and Table 1). The convulsive seizures lasted 115.0 ± 20.6 s, at a mean interval of 8.2 ± 1.4 min (Fig. 1F and Table 1). Non-convulsive seizures with Racine scale <4 also occurred also during phase 1 (Fig. 1E and Fig. S1A). Phase 2 was characterized by non-convulsive seizures featured with high-frequency spike-wave complexes (Fig. 1B–E). The spike frequency climbed from ~0.4 Hz to a peak 0.83 ± 0.07 Hz occurring at 9.0 ± 1.2 hours post KA infusion, and declined thereafter (Fig. 1D and Table 1). The spike frequency falling below 0.1 Hz marked the end of SE. The mean Racine scale of phase 2 was 2.1 ± 0.6 (Fig. 1G and Table 1). After phase 2, the video recordings indicated a gradual recovery of natural behavior, including free exploring, grooming, sniffing, and food consumption, along with EEG signals exhibiting the features of an interictal state.

Pan-adrenergic inhibition delays and shortens KA-induced status epilepticus

Adrenergic inhibition has previously been shown to boost glymphatic CSF influx[32,34,35]. An i.p. cocktail of adrenergic receptor antagonists (PPA: prazosin, propranolol and atipamezole) was administered immediately after the intrahippocampal KA infusion (KA-PPA, 5 min), while vehicle (isotonic saline) was injected in the control group (KA-Veh). In phase 1, PPA significantly postponed the onset of the first convulsive seizure (Fig. 1D–F and Fig. S1B). PPA treatment significantly prolonged the duration of individual seizures, the interval between seizures, and the duration of phase 1, but not the total number of seizures during phase 1 (Fig. 1F and Table 1). PPA treatment significantly shortened the duration of phase 2, and delayed the ascent of spike frequency (Fig. 1D, F). PPA significantly reduced the number of high-frequency spikes in phase 2 (Fig. 1F). PPA also significantly reduced the Racine scores of seizures in phase 1, but not in phase 2 (Fig. 1G). In summary, pan-adrenergic inhibition significantly delayed the initiation of SE, reduced the seizure severity during phase 1, and lowered the spike rate in phase 2. However, PPA did not alter the total number of seizures during phase 1.

Pan-adrenergic inhibition improves behavioral outcomes of KA-induced chronic epilepsy

The first dose of PPA given at five minutes post KA infusion (KA-PPA, 5 min) was followed by two subsequent doses at 24 h intervals (Fig. 2A). PPA significantly reduced KA-induced mortality rate during the first ten days post KA infusion as compared with KA-Veh mice (Fig. 2C). The PPA treatment also rescued the significant and persistent weight loss induced by KA (Fig. S7A,B). The PPA treatment on three consecutive days significantly reduced the spontaneous seizure severity at 3–4 weeks after the SE event, in terms of the number of convulsive seizures, the duration of individual seizure, and the maximal Racine scale scores (Fig. 2B,D). In fact, three of seven mice in the KA-PPA group did not exhibit any convulsive seizures during the recording sessions (Fig. 2B). In addition, PPA also significantly reduced the frequency of interictal spikes (KA-Veh 687.3 ± 48.2 vs KA-PPA 503.4 ± 73.9 spikes/h) (Fig. S3G). KA-Veh mice exhibited a decrease in the total distanced traveling in the open field test and a shorter latency to fall from the Rota-rod, but both deficits were normalized in the KA-PPA mice (Fig. 2E, F).

The total duration of SE lasts less than 30 h (Table 1). To avoid direct pharmacological manipulation during SE, we first applied the initial dose of PPA at 30 h post KA in a separate set of experiments (Fig. 3A). Much as in the KA-PPA (5 min) setting, the delayed PPA treatment (KA-PPA 30h) also significantly lowered the severity of convulsive seizures, in terms of the number of convulsive seizures, the maximal Racine scale scores and increased the number of convulsive seizure-free days (Fig. 3B, C). However, as distinct from KA-PPA (5 min) treatment, KA-PPA (30 h) did not shorten the mean duration of the convulsive seizures (Fig. 3C), nor did it rescue the

https://doi.org/10.1038/s41467-024-53430-y

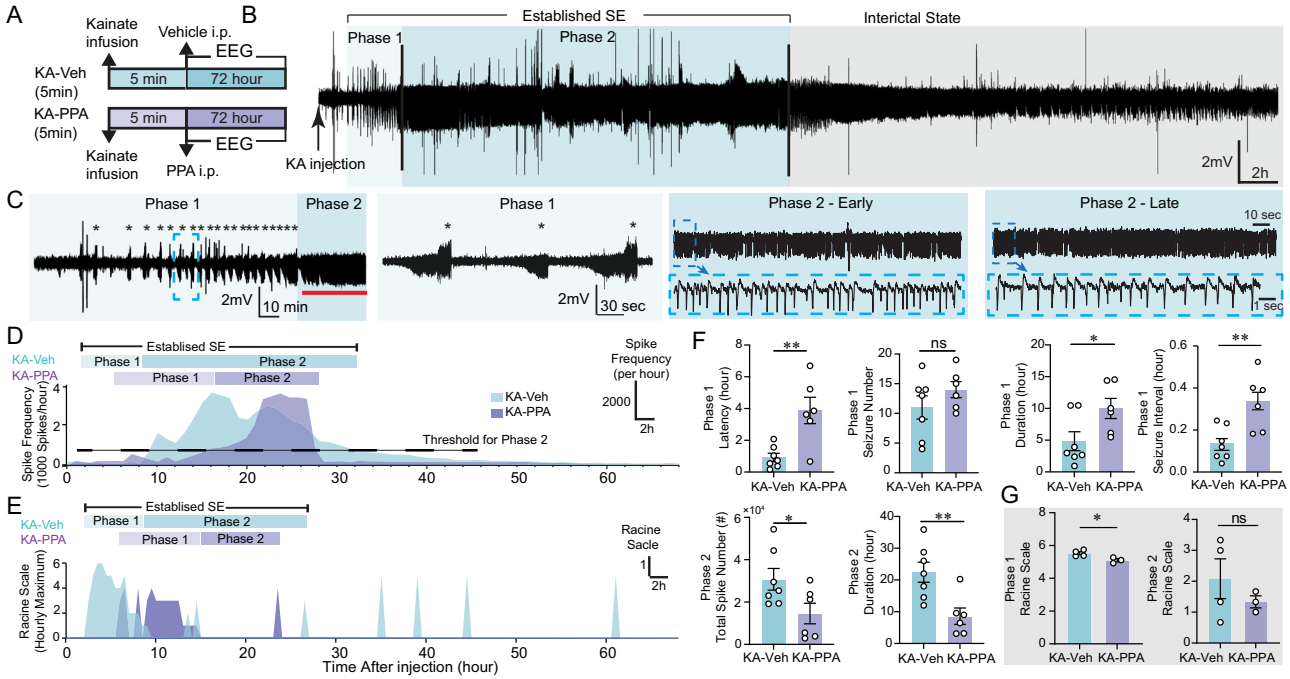

Fig. 1 | PPA changes the pattern of status epilepticus after intrahippocampal KA infusion. A Mice received an intrahippocampal infusion of KA (20 mM, 50 nl, 10 nl/min, right CA1 region) followed by continuous 72-hour EEG recordings. **B** EEG trace shows a representative example of KA-induced status epilepticus. **C** The epileptiform activity was subdivided into two characteristic phases: phase 1, the initial period, is characterized by recurrent seizures (stars), followed by phase 2 of continuous epileptiform spiking discharges (red line segment) with high frequency of spiking. Epileptiform discharges of phase 1 and phase 2 at higher temporal resolution are shown on the right. **D** Time-course spike frequency analysis of the KA-induced status epilepticus from representative vehicle and PPA-treated mice over 72 hours after intrahippocampal KA infusion. PPA is an i.p. pan-adrenergic receptor blocker cocktail consisting of prazosin (6 mg/kg), propranolol (6 mg/kg) and atipamezole (0.6 mg/kg). We chose a threshold of 0.1 Hz spike frequency for the termination of phase 2 (horizontal dash line). **E** Hourly maximum Racine scale by video inspection of KA-induced status epilepticus from representative vehicle- and PPA-treated mice after intrahippocampal KA infusion. **F** Histogram comparing the durations of the two phases of KA-induced status epilepticus in vehicle and PPA treated KA mice. KA-Veh ($n = 7$) versus KA-PPA ($n = 6$): Phase 1 latency of the first seizure post KA infusion, $^{**}P = 0.004$ (unpaired two-tailed t-test); seizure number, $P = 0.148$ (two-tailed Mann–Whitney test); Phase 1 duration, $^{*}P = 0.038$. (unpaired two-tailed t-test); Seizure interval, $^{**}P = 0.0011$ (unpaired two-tailed t-test). Phase 2, Total spike number, $^{*}P = 0.043$ (unpaired two-tailed t test); Phase 2 duration, $^{**}P = 0.007$ (unpaired two-tailed t-test). **G** In a subset of the mice, Racine scale was quantified from analysis of videotape recordings. KA-Veh ($n = 4$) versus KA-PPA ($n = 3$): Racine scores of Phase 1, $^{*}P = 0.029$ (unpaired two-tailed t-test); Racine scores of phase 2, $P = 0.380$ (unpaired two-tailed t-test). Data are presented as mean ± SEM.

body weight loss or mortality rate as compared with KA-Veh (Fig. S7D, E). Recordings were also conducted at two months post KA infusion after the delayed administration of PPA (Fig. 3D). At two months, the KA-PPA (30 h) group had a significant reduction in the number of convulsive seizures, but no difference in maximal Racine scale and number of convulsive seizure-free days at two months (Fig. 3E, F). In summary, the early three-day pan-adrenergic inhibition, initiated either at five minutes or 30 hours post KA infusion, effectively reduced the number of convulsive seizure occurrences in the chronic stages three weeks or two months later. Thus, three-day pan-adrenergic inhibition suppressed delayed epileptogenesis after the initial SE event.

Table 1 | Status Epileptics Parameters

Phase	Parameters	KA-Veh	KA-PPA	*p*-Value
Phase 1	Lag Time before First Seizure	0.9 ± 0.3 h	3.9 ± 0.8 h	0.004
	Duration of Phase 1	4.8 ± 1.5 h	10.0 ± 1.6 h	0.038
	Total Number of Seizures	10.1 ± 2.0	14.0 ± 1.4	0.142
	Duration of Seizures	115.0 ± 20.6 s	204.2 ± 17.3 s	<0.001
	Interval between Seizures	8.2 ± 1.4 min	20.3 ± 2.5 min	0.001
	Racine Scale (maximum hourly score)	5.5 ± 0.1	5.1 ± 0.1	0.029
Phase 2	Onset of Phase 2	5.7 ± 1.4 h	14.6 ± 1.4 h	0.001
	Duration of Phase 2	22.5 ± 3.2 h	8.6 ± 2.6 h	0.007
	Peak of Spike Frequency	0.8 ± 0.1 Hz	0.7 ± 0.1 Hz	0.201
	Time of Peak Frequency from KA infusion	9.0 ± 1.2 h	18.1 ± 2.2 h	0.003
	Racine Scale (maximum hourly score)	2.1 ± 0.6	1.3 ± 0.2	0.380
	Duration of Phase 1 + Phase 2	26.1 ± 4.2 h	19.9 ± 2.0 h	0.265

P-values were calculated by unpaired two-tailed t-test.

A single dose of PPA administered at the chronic phase exhibits a transient anti-epileptic effect

We next investigated the pharmacological effect of PPA administered at three weeks post KA (KA-PPA, 3 weeks) (Fig. 4A). A single dose of PPA significantly suppressed the number of convulsive seizures during the subsequent six hours, and delayed the onset of the first convulsive seizure (Fig. 4B, C). The numbers of convulsive seizures during the 12 h post-drug administration were comparable between PPA and Veh groups (Fig. S8), while the PPA treatment tended to shorten the duration of the convulsive seizures prevailing during this time window (Fig. 4C). In addition, PPA significantly suppressed the frequency of interictal spikes by ~40% between one and three hours post drug administration, as compared to the individual baseline rates before drug injection, while i.p. vehicle injection was without any such effect (Fig. 4D, E). In summary, a single dose of PPA applied at three weeks post KA infusion transiently suppressed spontaneous epileptic discharges in chronic epileptic mice.

https://doi.org/10.1038/s41467-024-53430-y

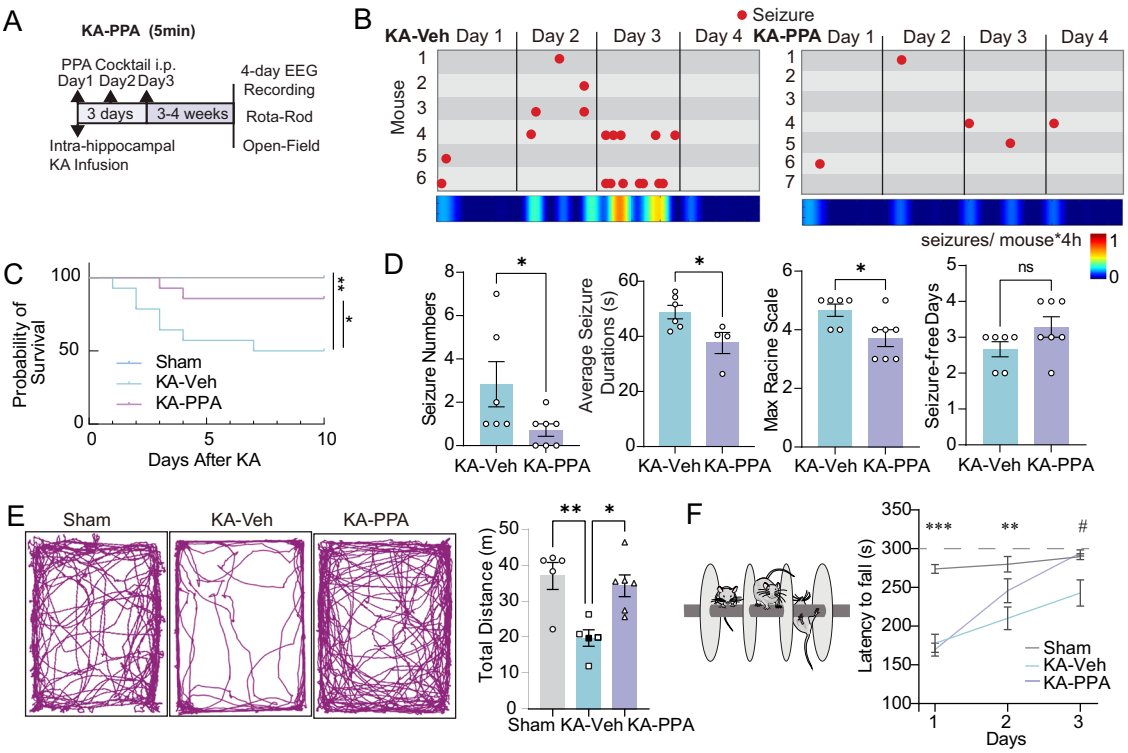

Fig. 2 | Pan-adrenergic inhibition improves behavioral outcomes of KA-induced chronic epilepsy. A Timeline of the experimental design. Five minutes after intrahippocampal KA infusion, mice were randomly divided into two groups that received daily injections of either PPA or vehicle for three consecutive days. After 3–4 weeks, cortical EEG electrodes were implanted in a subgroup of mice and EEG recordings obtained one week later. In parallel, we measured open-field and Rota-rod behavioral scores in a separate group of mice. **B** Seizure event plots show each convulsive seizure (red dot) onset time for individual mice in four-day recordings from the KA (left) and PPA-treated KA (right) groups. Heatmap (below) indicates the frequency of seizure onsets per mouse per four-hour recording in each group. **C** Kaplan–Meier survival curve of Sham, KA-Veh and KA-PPA (5 min) groups after KA infusion ($n = 12$ each, Sham vs KA-Veh $^{*}P = 0.039$, KA-Veh vs KA-PPA $^{**}P = 0.003$, Log-rank test). **D** The numbers of seizures in 4-day recordings, duration of spontaneous seizures, maximum Racine scale in four days, and number of seizure-free days contrasted between KA-Veh and KA-PPA mice. KA-Veh ($n = 6$) versus KA-PPA ($n = 7$). Seizure numbers, $^{*}P = 0.044$ (two-tailed Mann–Whitney test); seizure duration, $^{*}P = 0.031$ (unpaired two-tailed t-test); maximal Racine scale, $^{*}P = 0.048$ (two-tailed Mann–Whitney test) and seizure-free days, $P = 0.237$ (unpaired two-tailed t-test). **E** The representative traces of motion trails in the open-field test among Sham, KA-Veh and KA-PPA groups (left). The comparisons of total distances traveled are presented on the right. (one-way ANOVA, Tukey's multiple comparisons test, Sham ($n = 5$) vs KA-Veh ($n = 5$) $^{**}P = 0.006$, KA-Veh ($n = 5$) vs KA-PPA ($n = 6$) $^{*}P = 0.013$). **F** Motor coordination and motor learning by the Rota-Rod test showing partial recovery with PPA treatment. Comparison of the latency to fall among Sham, KA-Veh and KA-PPA groups (two-way ANOVA, Tukey's multiple comparisons test, Sham ($n = 7$) vs KA-Veh ($n = 8$), $^{***}P < 0.001$, $^{**}P = 0.005$; KA-Veh ($n = 8$) vs KA-PPA ($n = 8$) $\#P < 0.05$). Data are presented as mean ± SEM.

Pan-adrenergic inhibition enhances glymphatic influx in healthy and epileptic mice

PPA boosts glymphatic transport in anesthetized mice[32,34]. In the present study, PPA enhanced the glymphatic influx by 47.7% in coronal slices at AP + 0.6 mm in awake, *wildtype* mice (Fig. 5A,B). PPA significantly increased the glymphatic influx in ventral cerebral cortex and hypothalamus ROIs as compared with WT-Veh mice AP -1.2 mm (Fig. 5C). PPA also significantly elevated the EEG slow wave activity (SWA, 0.5–4 Hz) (Fig. 5D). PPA treatment administered immediately following KA intrahippocampal infusion rescued the significant reduction on glymphatic influx otherwise seen at five hours after intrahippocampal KA infusion, in the midst of phase 1 of the established SE (AP + 0.6 mm, Fig. 5E,F). However, the brain regional quantification showed no significant restoring effect by PPA of glymphatic influx in individual regions (Fig. S2B,C). PPA administered at three weeks post KA infusion exhibited similar effects in rescuing the suppression of glymphatic influx in KA-Veh mice (AP + 0.6 mm, Fig. 5G,H). Brain regional enhancement of glymphatic influx in these animals was similar to the effect of PPA in *wildtype* mice (Fig. 5C,I). In chronic epileptic mice, PPA significantly enhanced EEG slow wave activity (0.5–4 Hz) and reduced the power of theta band (4–8 Hz) (Fig. 5J). These observations extend the prior findings that SWA correlates positively with glymphatic tracer influx[32,44].

Early pan-adrenergic inhibition improves glymphatic function in the chronic epileptic stage

Based on the observations of the improvements in epileptogenesis and behavioral outcomes in KA mice receiving early three-day PPA treatment (Fig. 2), we next tested if early PPA treatment also improves glymphatic function in chronic epileptic mice (Fig. 6A). Glymphatic influx was significantly lower in KA-Veh mice compared to control mice, but was fully rescued by early PPA treatment (Fig. 6B). We also assessed glymphatic efflux with a real-time in vivo assay, following a recently published protocol[45]. Here, we imaged the femoral vein lumen for up to two hours following intrastriatal infusion of the small molecular weight (0.96 kDa) fluorescent tracer Direct Blue 53 (DB53) in anesthetized mice (Fig. 6C). DB53 binds irreversibly to blood albumin, such that the blood signal represents the total export of DB53 from the brain to blood[45]. There was a significant reduction in DB53 fluorescence intensity over the femoral vein in chronic KA mice, indicating suppressed glymphatic efflux. The mice with early PPA treatment exhibited efflux levels similar to sham mice, suggesting a complete rescue of glymphatic efflux by PPA (Fig. 6D).

AQP4 facilitates glymphatic flow and is selectively expressed by astrocytes in brain[46,47], being mainly present in the astrocytic endfeet that surround the vasculatures, whereas loss of this vascular polarization is linked to reduced glymphatic fluid transport[28]. KA-Veh mice

https://doi.org/10.1038/s41467-024-53430-y

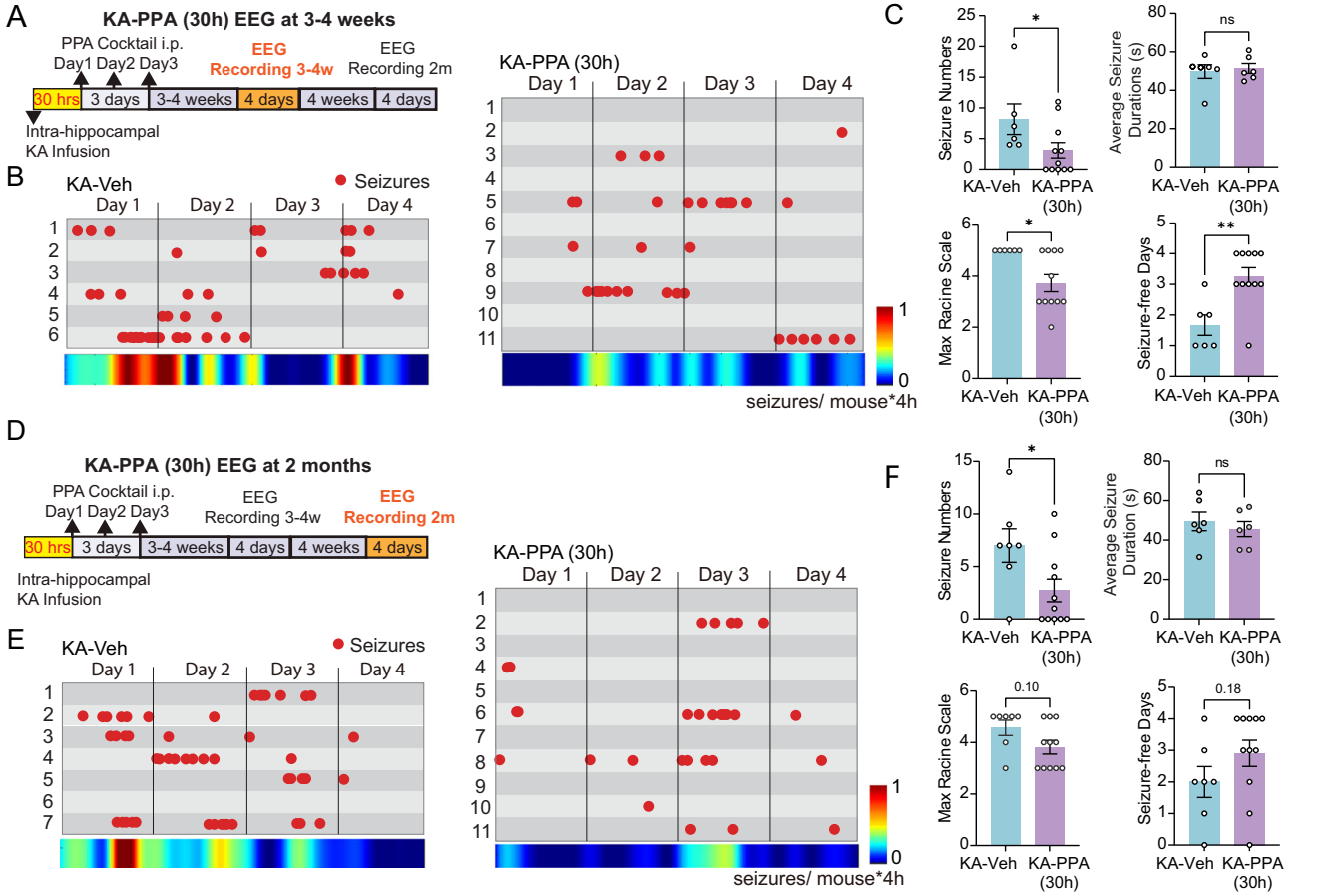

Fig. 3 | 30-hour delayed pan-adrenergic inhibition reduces rate of spontaneous seizures in a chronic epilepsy model. A Timeline of experimental design. At 30 h after intrahippocampal KA infusion, mice were randomly divided into two groups that received either a daily injection of PPA or vehicle for three consecutive days. After 3–4 weeks, cortical EEG electrodes were implanted and recordings were obtained one week later. **B** Seizure event plots show each convulsive seizure (red dot) onset time for individuals in four-day recordings from the KA-Veh (left) and KA-PPA (30 h) (right) groups. Heatmap (below) indicates the frequency of seizure onsets per mouse per four-hour recording in each group. **C** The analysis of seizure numbers, duration of spontaneous seizures, maximum Racine scale in the four-day recordings, and seizure-free days between the KA-Veh and KA-PPA (30 h) mouse groups at 3–4 weeks. KA-Veh ($n = 6$) versus KA-PPA ($n = 11$), maximal Racine scale, $^{*}P = 0.031$ (two-tailed Mann–Whitney test); seizure numbers, $^{*}P = 0.042$ (two-tailed Mann–Whitney test); average seizure duration, $P = 0.719$ (unpaired two-tailed *t*-test), and seizure-free days, $^{**}P = 0.004$ (two-tailed Mann–Whitney test). **D** Timeline of experimental design. At two months post-KA infusion, four-day EEG recordings were obtained from the KA-Veh and KA-PPA (30 h) groups. **E** Seizure event plots show each convulsive seizure (red dot) onset time for individuals in the 4-day recordings from the KA-Veh (left) and KA-PPA (30 h) (right) groups at two months. **F** The heatmap (below) indicates the frequency of seizure onset per mouse during the four-hour recordings in each mouse group. The analysis of seizure numbers, duration of spontaneous seizures, maximum Racine scale in the four-day recordings, and seizure-free days between the KA-Veh and KA-PPA (30 h) mouse groups at two months. KA-Veh ($n = 7$) versus KA-PPA ($n = 11$), maximum Racine scale, $P = 0.100$ (two-tailed Mann–Whitney test), seizure numbers, $^{*}P = 0.035$ (unpaired two-tailed *t*-test); average seizure duration, $P = 0.535$ (unpaired two-tailed *t*-test), and seizure-free days, $P = 0.181$ (unpaired two-tailed *t*-test). Data are presented as mean ± SEM.

exhibited a significant upregulation of AQP4 protein expression levels in the hippocampal CA1 region and decreased vascular polarization in multiple brain regions at three weeks post KA infusion (Fig. S3C–E, Fig. 6E,F). There was a significant reduction in AQP4 polarization in somatosensory and ventral cortex, and hypothalamus of KA-Veh mice (Fig. S3A–D), but a partial normalization was evident in the KA-PPA group (Fig. S3D). In summary, early PPA treatment increased glymphatic clearance and partially normalized AQP4 vascular polarization in the chronic epileptic phase.

Early pan-adrenergic inhibition alleviates the delayed inflammatory responses

At three weeks post KA infusion, there was increased expression of the astrocytic marker GFAP (astrocyte marker) and the microglial marker CD68 in the hippocampal CA1 and somatosensory cortex (S1) in KA-Veh mice compared to Sham-Veh mice (Fig. S4A,B). The KA-PPA (5 min) treatment significantly reduced GFAP-positive area in both regions, whereas CD68 positive area increased only in the hippocampus of the KA-Veh group, with no effect of PPA in chronic KA mice (Fig. S4A,B). Neuronal loss was evident in the hippocampus and somatosensory cortex in KA-Veh mice to NeuN immunohistochemistry, but PPA treatment significantly reduced the neuronal loss (Fig. S4C). We also sampled the extracellular fluid via cerebral microdialysis and measured cytokine/chemokine levels three weeks post KA infusion (Fig. S5A). Concentrations of the pro-inflammatory cytokines, G-CSF, IL-1β, IL-6 and the pro-inflammatory chemokine KC (CXCL1) were significantly higher in KA-Veh mice versus Sham-Veh mice. PPA treatment significantly lowered the levels of G-CSF as compared with KA-Veh mice (Fig. S5B–D).

Glymphatic influx correlates inversely with the severity of epilepsy

We correlated CSF tracer influx with the severity of the spontaneous seizure and with indices of cerebral pathology (GFAP immunolabeling, neuronal density, and AQP4 vascular polarization) three weeks after KA infusion. The correlation analysis showed that glymphatic CSF

https://doi.org/10.1038/s41467-024-53430-y

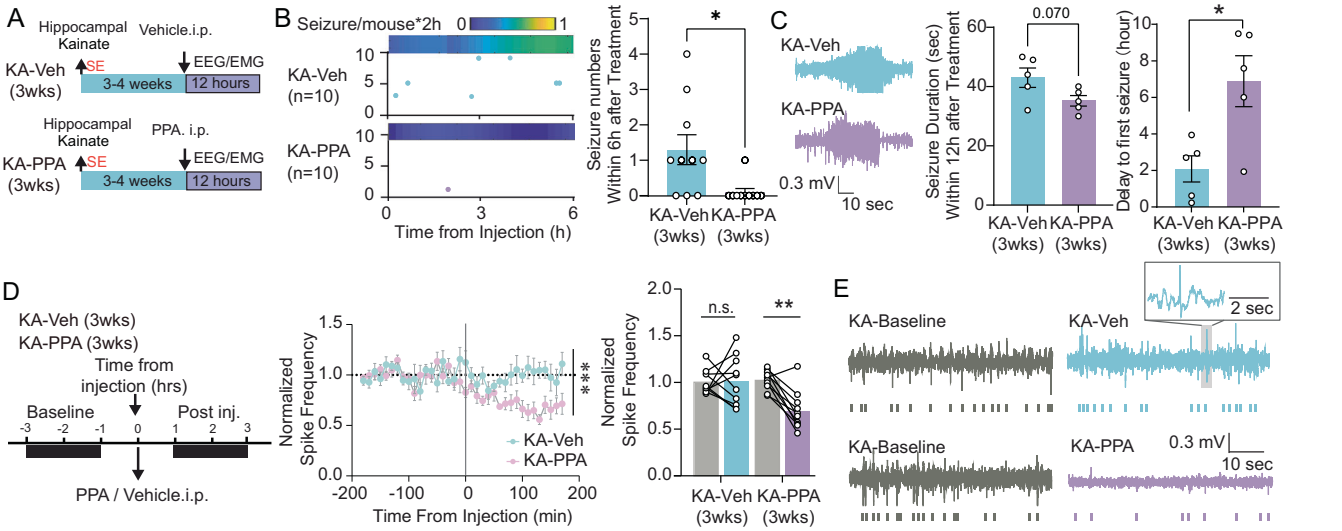

Fig. 4 | Delayed administration of PPA at 3 weeks post-KA transiently reduces seizure burden. A Timeline of experimental design of 3-week delayed PPA treatment. At 3–4 weeks post KA infusion, mice received a single intraperitoneal dose of PPA or saline vehicle. (**B**) Representative plot of seizures onset distributions during the first six hours after PPA or vehicle i.p. Each horizontal line represents a mouse and each dot indicates a seizure. The heatmap above indicates the seizure frequency of each group (left). The number of spontaneous convulsive seizures (middle), $N = 10$ each, $^{*}P = 0.013$, two-tailed Mann–Whitney test. **C** For both KA-Veh and KA-PPA groups, five out of ten mice had convulsive seizures during 12-hour recording session. The average duration of convulsive seizures (left) and the delay to the first seizure (right) is summarized ($n = 5$ each, seizure duration, $P = 0.070$, unpaired two-tailed t-test; delay to the first seizure, $^{*}P = 0.016$, unpaired two-tailed t-test). **D** Timeline and normalized spike frequency is calculated based on the pre-PPA or -vehicle baseline (left). Quantification between two-hour window preceding and after PPA or vehicle injection. (Middle, $n = 10$ each, time-treatment interaction, 2-way ANOVA, $^{*}P < 0.001$. Right, $n = 10$ each, 2-way ANOVA, Sidak's multiple comparisons test. $^{**}P = 0.002$). **E** Representative traces demonstrating interictal spikes before and after PPA or vehicle treatment in epileptic mice. Data are presented as mean ± SEM.

tracer influx correlated inversely with spike frequency ($R^2 = 0.664$, $p < 0.001$), seizure duration ($R^2 = 0.874$, $p < 0.001$) and number of seizures ($R^2 = 0.394$, $p = 0.004$), and with the severity of astrogliosis ($R^2 = 0.827$, $p < 0.001$). On the other hand, glymphatic CSF tracer influx correlated positively with the AQP4 polarization index ($R^2 = 0.342$, $p = 0.022$), and CA1 hippocampal neuronal density ($R^2 = 0.822$, $p < 0.001$) (Fig. 6G). Taken together, the CSF glymphatic inflow closely correlates with the severity of epileptiform discharges and brain pathologies in the chronic phase of intrahippocampal KA-induced epilepsy.

Aqp4 knockout aggravated KA-induced SE and the severity of chronic epilepsy

We next tested whether a constitutive reduction in glymphatic flow would worsen the outcome in KA-induced epilepsy. *Aqp4* knockout (*Aqp4*$^{-/-}$, *Aqp4*-KO) mice on a C57BL/6 background have previously been shown to exhibit reduced glymphatic flow[28,30]. KA-Veh *Aqp4* knockout mice and their *wildtype* littermates exhibited similar neuronal discharges patterns as the FVB mice used in the prior experiments (Figs. 1 and 7A). As compared with *wildtype* littermate controls, *Aqp4*-KO mice exhibited significantly shortened latency of first seizure onset, greater mean duration and severity of seizure onset in phase 1, and prolonged the duration and total epileptic spike number in phase 2 (Fig. 7B). *Aqp4*-KO mice tended to have longer latency to phase 2 (Fig. 7B,C). There was no significant difference in the number of seizures in *Aqp4*-KO mice compared to controls in Phase 1 (Fig. 7C). In several epilepsy models, C57BL/6 strain background mice develop less severe seizures than FVB mice[48,49]. Similarly, we here observed that four of five *wildtype* mice did not exhibit spontaneous seizures during the four consecutive days of recording in the chronic phase (Fig.7D). In contrast, the *Aqp4* knockout mice exhibited a significantly higher number of seizures, prolonged seizure duration, higher maximal Racine scale readouts and fewer seizure-free days in the chronic phase as compared with *wildtype* littermates (Fig. 7D).

Discussion

Several lines of evidence suggest that early intervention during a status epilepticus (SE) attack is critically important for long-term prognosis[50–53]. In this study, we report that administering a cocktail of pan-adrenergic receptor antagonists (designated as PPA) to mice in the acute phase of SE was beneficial with respect to epileptic, behavioral, and pathological outcomes in the chronic phase. PPA administered five minutes after the intrahippocampal KA infusion did not reduce the number of convulsive seizures, but delayed their onset (Fig. 1). Three-consecutive days' treatment of PPA after KA infusion efficiently reduced the epileptic discharges and improved performance on behavioral tests, as well as brain pathology outcomes (Fig. 2 and S3, S4). Early PPA treatment in seizure mice also improved glymphatic transport and restored the AQP4 vascular polarization (Figs. 5, 6, and S3). Delaying the initial dose of PPA treatment until immediately after the cessation of SE, or even by 30 h after KA infusion, also imparted long-term benefits, including a reduction in the number of seizures and a higher number of seizure-free days at three weeks and two months after KA infusion (Fig. 3). This observation is important, because it shows that PPA administered after SE attenuates the long-term severity of KA-induced epilepsy.

A single dose of PPA administered in the chronic epileptic phase (three weeks) also transiently reduced the number of spontaneous seizures and lowered the interictal spike frequency (Fig. 4). In contrast, *Aqp4* knockout mice with suppressed glymphatic transport, exhibited a significantly prolonged duration of status epilepticus and more severe epileptic discharges in chronic phase (Fig. 7). These findings support the notion that the enhancement of glymphatic function by pan-adrenergic receptor antagonism could be a potential approach for alleviating epileptogenesis.

Pan-adrenergic inhibition reduces KA-induced status epilepticus

Adrenergic receptors are known to regulate neuronal excitability[54–58]. Excessive NE release occurs in the setting of SE[59], and clinical and pre-

https://doi.org/10.1038/s41467-024-53430-y

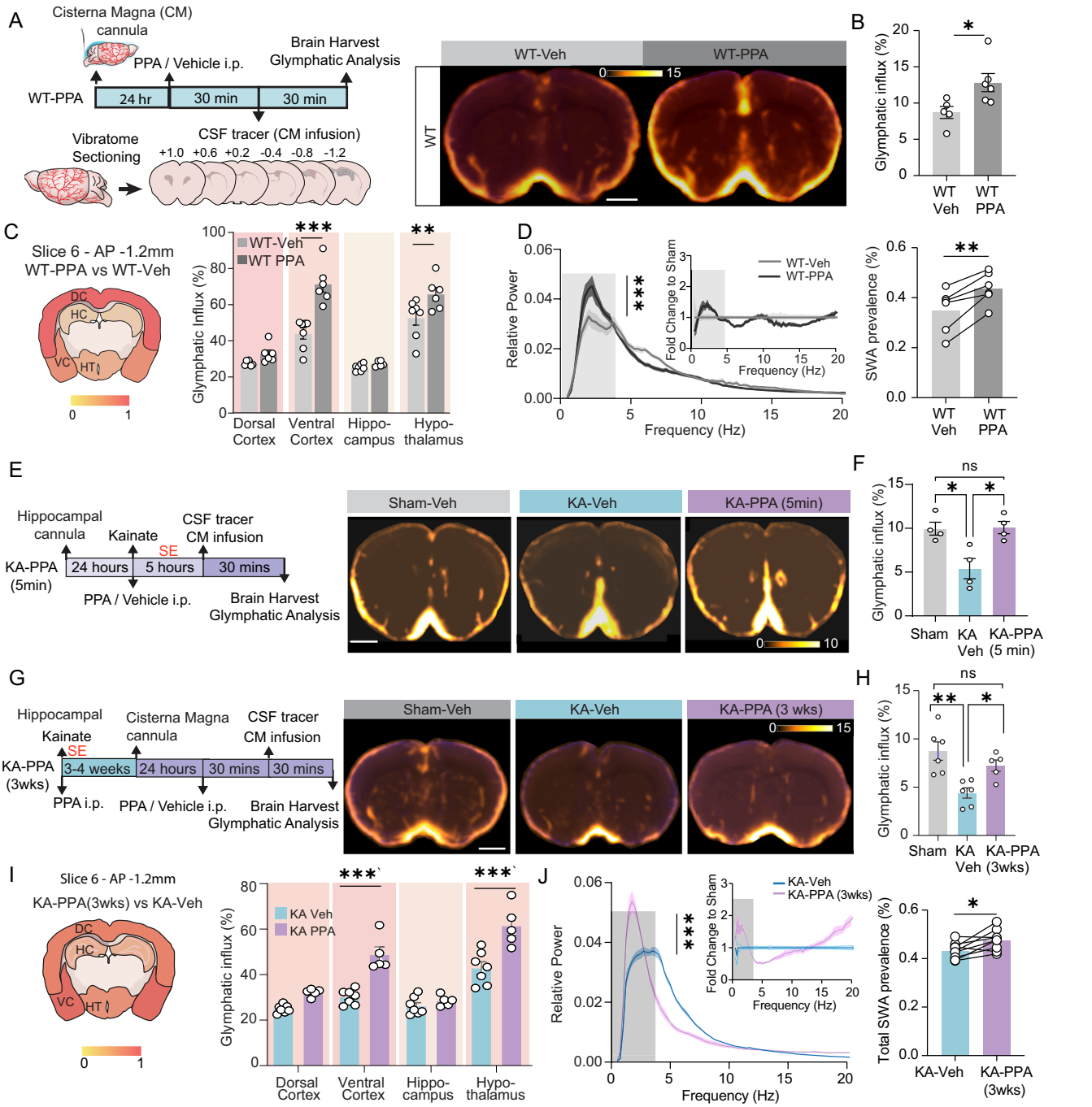

Fig. 5 | PPA treatment enhances acute and chronic glymphatic tracer influx, while increasing EEG slow wave activity. A Experimental design (Left) and population-based average images of tracer distribution (right). **B** The CSF tracer influx area in brain slices (AP + 0.6 mm), WT-Veh ($n = 5$) vs WT-PPA ($n = 6$), unpaired two-tailed t-test, $^{*}P = 0.028$. **C** Regional influx analysis in brain slices (left, AP −1.2 mm) after PPA in *wildtype* mice. Histograms summarizing the glymphatic influx area fractions in multiple brain regions (right, AP -1.2 mm). WT-Veh ($n = 7$) vs WT-PPA ($n = 6$), two-way ANOVA, Sidak's multiple comparisons test. Ventral cortex, $^{***}P < 0.001$, hypothalamus, $^{**}P = 0.008$. **D** EEG power spectrum analysis in *wildtype* mice. Left, raw EEG spectrum, $n = 6$ each, $^{***}P < 0.001$, time-treatment interaction, two-way ANOVA. Insert, fold change to WT-Veh. Right, slow wave activity (SWA, 0.5–4 Hz), $n = 6$ each, $^{**}P = 0.004$, paired two-tailed t-test. **E** Experimental design (left) and population-based images of coronal sections (right, AP + 0.6 mm). **F** The glymphatic influx area fractions in slices (AP + 0.6 mm), $n = 4$ each, Sham-Veh vs KA-Veh, $^{*}P = 0.014$, KA-Veh vs KA-PPA, $^{*}P = 0.012$, one-way ANOVA, Tukey's multiple comparisons test. **G** Experimental design (left) and Population-based images of brain coronal sections (right, AP + 0.6 mm). **H** The glymphatic influx area fractions in slices (AP + 0.6 mm), Sham-Veh ($n = 6$) vs KA-Veh ($n = 6$) $^{**}P = 0.002$, KA-Veh ($n = 6$) vs KA-PPA (3 wks) ($n = 5$) $^{*}P = 0.043$, one-way ANOVA, Tukey's multiple comparisons test. **I** Regional influx analysis in brain slice (AP −1.2 mm) after PPA in chronic epileptic mice. KA-Veh ($n = 7$) vs KA-PPA ($n = 5$). Ventral cortex, $^{***}P < 0.001$, hypothalamus, $^{***}P < 0.001$, two-way ANOVA, Sidak's multiple comparisons test. **J** EEG power spectrum in KA mice. Left, raw EEG spectrum, $n = 6$ each, $^{***}P < 0.001$, time-treatment interaction, two-way ANOVA. Insert, fold change to KA-Veh. Right, the total SWA power (0.5–4 Hz). Scale bar = 1 mm. Data are presented as mean ± SEM.

https://doi.org/10.1038/s41467-024-53430-y

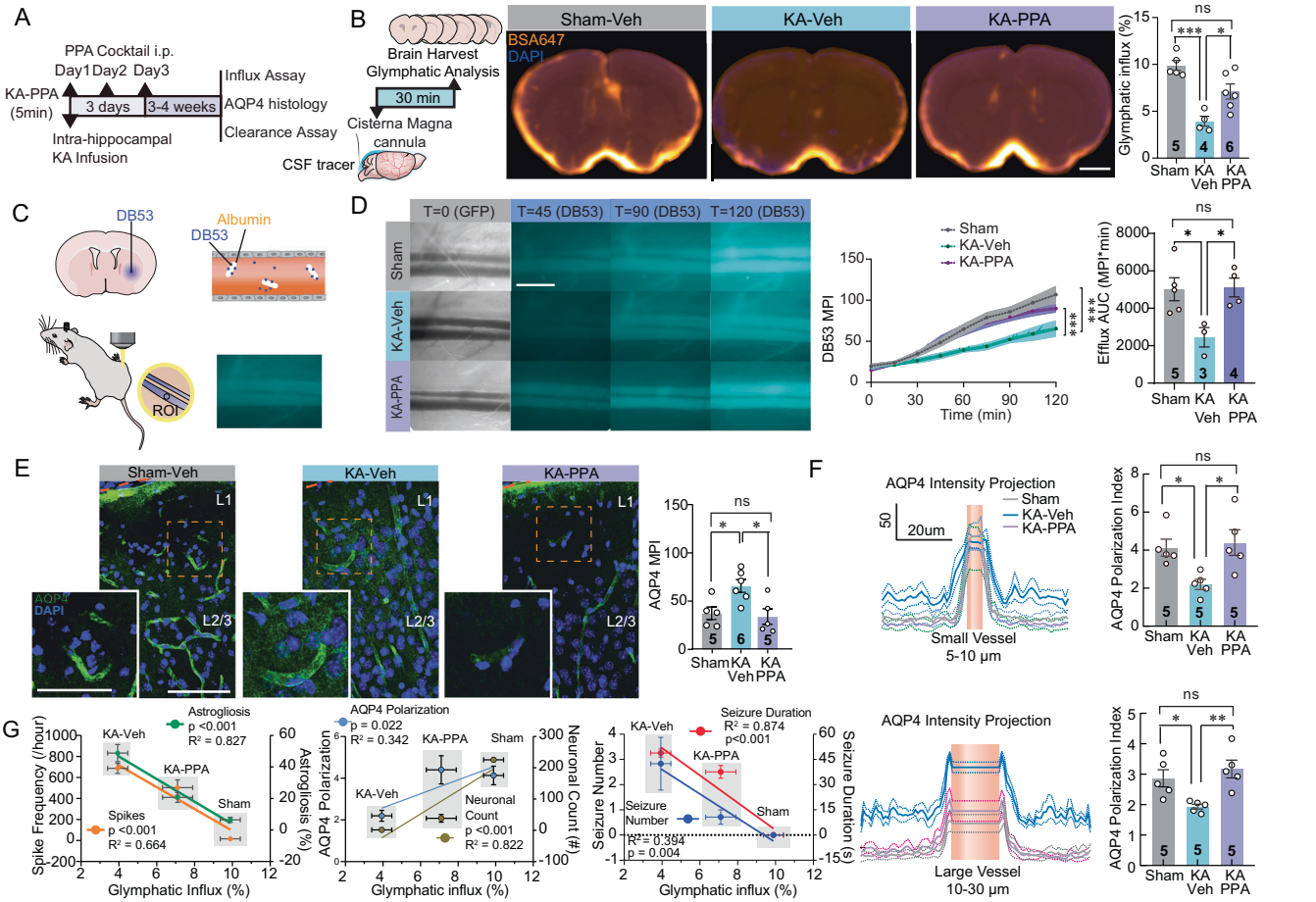

Fig. 6 | Early PPA treatment results in improved glymphatic transport in the epilepsy chronic phase. A At 3–4 weeks, AQP4 immunostaining, CSF tracer influx and clearance were analyzed. **B** Glymphatic analysis (left). Population-based average images of CSF tracer distribution in coronal sections (AP + 0.6 mm) (middle). The tracer influx area fractions (right), sham-Vehicle vs KA-Vehicle ***$P < 0.001$, KA-Vehicle vs KA-PPA *$P = 0.020$, One-way ANOVA, Tukey's multiple comparisons test. **C** Schematic showing striatal cannula implantation and in vivo DB53 measurement. **D** Representative in vivo femoral vein images. (Left, scale-bar,1 mm). Time-course fluorescent intensity of DB53 in the femoral vein (middle, Sham ($n = 5$) vs KA-Veh ($n = 3$), ***$P < 0.001$; KA-Veh ($n = 3$) vs KA-PPA ($n = 4$), ***$P < 0.001$). Quantification of efflux (area under curve, AUC, 0-120 min) (right, Sham vs KA-Veh *$P = 0.035$, KA-Veh vs KA-PPA *$P = 0.037$, one-way ANOVA, Tukey's multiple comparisons test). **E** AQP4 expression in somatosensory cortex, insert show higher magnification images (scale bar, 80 µm, insert, 50 µm). Quantification of AQP4 immunoreactivity (Sham-Veh KA-Veh *$P = 0.032$, KA-Veh vs KA-PPA *$P = 0.017$, one-way ANOVA, Tukey's multiple comparisons test). **F** Quantification of AQP4 polarization index around small and large vessels (Upper panel, small vessels, sham-Veh vs KA-Veh, *$P = 0.040$; KA-Veh vs KA-PPA, *$P = 0.020$. Lower panel, large vessels, Sham-Veh vs KA-Veh *$P = 0.042$, KA-Veh vs KA-PPA **$P = 0.008$. One-way ANOVA, Tukey's multiple comparisons test). **G** Glymphatic tracer influx correlates with the severity of epilepsy. Left, Correlations of CSF tracer influx with interictal spike frequency ($R^2 = 0.664$, ***$P < 0.001$), and with the severity of astrogliosis by CA1 GFAP expression ($R^2 = 0.827$, ***$P < 0.001$). Middle, correlations of influx with CA1 neuronal count ($R^2 = 0.822$, ***$P < 0.001$), and cortical AQP4 polarization index ($R^2 = 0.342$ *$P = 0.022$). Right, Correlations of influx with seizure duration ($R^2 = 0.874$, ***$P < 0.001$) and seizure number ($R^2 = 0.394$, **$P = 0.004$). Linear least squares regression. MPI, mean pixel intensity. Mice/group n are indicated on the graph. Data are presented as mean ± SEM.

clinical evidence indicates that adrenergic receptor subtypes moderate the susceptibility of epileptic seizures. A 2010 review summarized the effect of antidepressants and adrenergic medications such as clonidine, prazosin, and propranolol on seizure susceptibility and epilepsy development. The author argued that all three major subtypes of adrenergic receptors had both anti- and pro-seizure effects[60]. Another 2016 review organized the previous reports by the category of evidence and type of seizures[61]. The authors concluded that in human studies, α_1 receptor hyposensitivity contributed to the failed inhibition of focal seizures, whereas β-receptor activation enhanced the anticonvulsive efficacy of conventional anti-epileptic drugs. In animal models of focal seizure, α_{1A}, α_2, and β_2-receptor stimulation inhibited seizures, while α_{1D} receptor antagonism exerted an anti-seizure effect. In generalized seizure models, most data suggest that α_1-and α_2-receptor agonists have anticonvulsant actions, but that β-receptor antagonists also have anticonvulsant activity. Several recent studies also support a protective role of adrenergic signaling in seizures. Clinically, α_{2B} receptor mutations are associated with autosomal dominant cortical myoclonus and epilepsy (ADCME)[62]. In experimental studies, α-adrenergic receptors mediate the inhibitory effect of electrical brain stimulation on epileptiform activity[63]. Animal studies suggest that β_{2A}-receptor activation prevents bicuculline-induced seizure in the piriform cortex[64]. Ex vivo studies revealed that β-receptor activation shortened and delayed spike bursts evoked by 4-aminopyridine in hippocampal slices[65]. Finally, activation of α_{2A} receptors inhibited seizure-like activity in a brain slice picrotoxin model[66]. Overall, drugs targeting adrenergic receptor subtypes have exerted a variety of effects on seizures in preclinical and clinical studies.

We here hypothesize that blocking all the main subtypes of adrenergic receptors might reduce the severity of the initial SE, based on our observations that the same treatment potently enhanced glymphatic transport[32], and was neuroprotective in acute ischemic stroke and traumatic brain injury models[34,35]. Hyperexcitability during SE is believed to be the key mediator of

https://doi.org/10.1038/s41467-024-53430-y

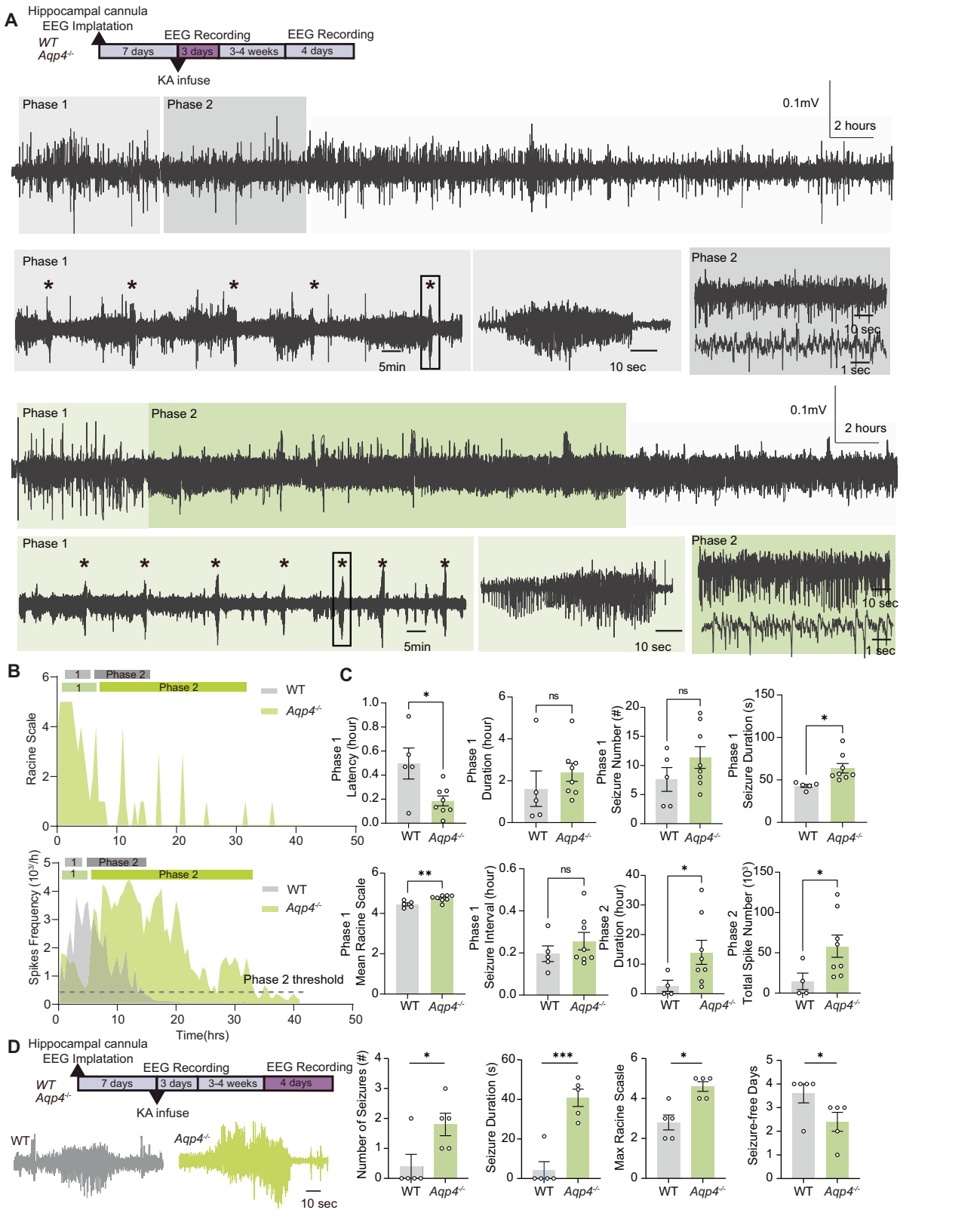

neuronal loss and remodeling of synaptic networks leading to recurrent spontaneous seizures[67–70]. Based on the rational, that enhancing glymphatic clearance would improve the normalization of extracellular K^{+}[34] and lactate[71] and flush other mediators of hyperexcitability from the brain, we here tested the effects of PPA on glymphatic function and epileptogenesis. To map the effect of pan-adrenergic blockage, we employed long-term EEG/EMG/video recordings (three days) after intra-hippocampal KA infusion. In phase 1, PPA delayed the seizure onset and increased the inter-seizure intervals, thereby increasing the duration of seizure-free periods. In phase 2, PPA triggered a substantial reduction in the average spike intensity and promoted normalization of spike activity. PPA also improved glymphatic fluid transport at five hours after KA infusion or during phase 2 SE in both groups (Fig. 5E).

Fig. 7 | AQP4 deletion aggravates KA-induced seizures. A AQP4-KO and C57 *wildtype* control mice received an intrahippocampal infusion of KA followed by continuous 72-hour EEG recordings. After 3–4 weeks, the same groups of mice underwent four-day EEG recordings. EEG trace shows a representative example of KA-induced status epilepticus (stars: seizures). As in Fig. 1, the epileptiform activity was subdivided into two phases, with depiction of recurrent seizure onsets in phase 1 (middle in light-colored box). Epileptiform discharges of phase 2 are displayed at higher temporal resolution (right in dark-colored box). **B** Time-course spike frequency and hourly maximal Racine scale of the KA-induced status epilepticus from representative WT and Aqp4-KO mice. **C** Histogram comparing the durations of the two phases of KA-induced status epilepticus in control and AQP4-KO mice. Phase 1, latency of the first seizure post KA infusion, WT ($n = 5$) versus Aqp4-KO ($n = 8$), $^{*}P = 0.019$, unpaired two-tailed *t*-test test; number of seizures, WT ($n = 5$) versus Aqp4-KO ($n = 8$), $P = 0.302$, unpaired Mann–Whitney's test; Phase 1 duration, WT ($n = 5$) versus Aqp4-KO ($n = 8$), $P = 0.378$, unpaired two-tailed *t*-test; seizure duration, WT ($n = 5$) versus Aqp4-KO ($n = 8$), $^{*}P = 0.017$, unpaired two-tailed *t*-test; seizure interval, WT ($n = 5$) versus Aqp4-KO ($n = 8$), $P = 0.343$, unpaired two-tailed *t*-test; mean Racine Scale, $^{**}P = 0.007$, unpaired two-tailed *t*-test. Phase 2, duration, WT ($n = 4$) versus Aqp4-KO ($n = 8$), $^{*}P = 0.026$, two-tailed Mann–Whitney's test; total spike number, WT ($n = 4$) versus Aqp4-KO ($n = 8$), $^{*}P = 0.047$, two-tailed Mann–Whitney's test. **D** The seizure numbers in the four-day recordings, duration of spontaneous seizures, maximal Racine scale in the four-day recordings, and seizure-free days compared between control and AQP4-KO mice during chronic epilepsy (3–4 weeks after intrahippocampal KA infusion). $N = 5$ each, seizure numbers, $^{*}P = 0.040$ (two-tailed Mann–Whitney's test); seizure duration, $^{***}P < 0.001$ (unpaired two-tailed t-test); maximal Racine scale, $^{*}P = 0.024$ (two-tailed Mann–Whitney's test) and seizure-free days, $^{*}P = 0.040$ (two-tailed Mann–Whitney's test). Data are presented as mean ± SEM.

Epileptogenesis and the partial rescue by pan-adrenergic blockage

The latency between the onset of acquired epilepsy and the initial insult is variable, with clinical reports ranging from months to years[72–74]. In the mouse model of intrahippocampal KA infusion, the animals develop spontaneous seizures with a frequency of 8.0 ± 6.3 per day after a latent period of 13–30 days[37,75–79]. In the latent period, epileptogenesis involves multiple and complex molecular and cellular mechanisms. According to the current literatures on human and rodent studies, epileptogenesis involves neurons and glial cells and is the downstream result of hypoxia[80,81], oxidative stress[82,83], and glutamate-mediated excitotoxicity[84–86]. Activation of glial cells as well as blood-borne inflammatory cell infiltration contribute to intracerebral release of inflammatory mediators such as cytokines that may cause secondary neuronal injury[84,87,88]. Breaching of the BBB and deficits in astrocytic K^+ buffering are additional factors in epileptogenesis[89,90]. Several lines of evidence suggest that axonal growth/sprouting, excitatory synaptogenesis, dendrite arborization and neurogenesis play crucial roles in rewiring neuronal circuits, which in turn facilitate electrical discharges that generate recurrent spontaneous seizures[91–93]. Adrenergic α- and β-receptors in the brain mediate pro- and anti-inflammatory responses under various conditions[94]. In our study, PPA exerted a clear anti-inflammatory role by dampening astrogliosis and increasing pro-inflammatory cytokine levels after KA infusion. Cytokines that are mainly released by microglia, including G-CSF which was suppressed by PPA, even though CD68 expression was unaffected. These observations suggest that PPA targeted select inflammatory pathways in microglial cells[95,96]. Additionally, our assessment of BBB permeability indicated that PPA did not significantly impact BBB integrity at the late phase of SE (24 h after SE, Fig. S6). We propose that boosting glymphatic fluid transport with PPA restricted the inflammatory response by promoting the clearance of lactate, K^+, cytokines and other agents promoting excitability[71,97] independent of changes in BBB permeability, with additional benefits obtained via adrenergic reguation of inflammatory cells. This also explains why, even though we did not find significant glymphatic enhancement in the hippocampus (Fig. 5C,I), probably due to severe astrogliosis as result of kainite acid local infusion[98,99], PPA treatment beneficial effects on epileptogenesis may reflect an improvement of brain-wide clearance[100].

Why does seizure activity reduce glymphatic influx and why does enhancing glymphatic flow shorten seizure duration?

Cerebrospinal fluid transport is propelled by several physiological drivers[101]. Along the glymphatic pathway, the influx is highly sensitive to changes in the extracellular space volume[32], which shrinks by approximately 35% during epileptic seizures[102,103]. Indeed, pilocarpine-induced seizures progressively shrank the extracellular space volume, which only slowly normalized along with the normalization of EEG activity in rats[104]. Shrinkage of the extracellular space volume increases tissue resistance towards fluid flow and reduces thereby glymphatic activity[27]. Thus, the suppression of glymphatic fluid transport in the acute phase of a seizure might be a consequence of cell swelling and extracellular space volume shrinkage. In the chronic phase of epilepsy, reactive gliosis and associated loss of perivascular polarization of AQP4 (Figs. 6E and S3) may plausibly be held responsible for sustained suppression of the glymphatic system. Thus, the depolarization of AQP4 in the chronic epileptic brain is likely a consequence of epileptic injury that contributes to glymphatic dysfunction. The more severe epilepsy exhibited by *Aqp4* knockout mice in the chronic phase gives support for a causative role of glymphatic function in aggravating epileptogenesis. This observation (Fig. 7) is in line with prior studies reporting a loss of AQP4 aggravates seizure severity and epileptogenesis[105,106]. Herein, we propose that AQP4-mediated glymphatic substance clearance is a relevant factor, although we do not exclude the possibility that other mechanisms such as edema formation and neuroinflammation[107,108] might increase the vulnerability of the brain following SE. It should also be noted that *Aqp4* knockout mice display several adaptive changes, including an expansion of the extracellular space volume, altered diffusion parameters and changes in astrocytic volume regulation and Ca^{2+} signaling[30,108–110]. In addition to the low glymphatic activity, these changes may contribute worsening of the KA-induced seizure in *Aqp4* knockout mice.

Another key question is why pan-adrenergic blockage prolonged phase 1 and thereby delayed the onset of phase 2 after intrahippocampal KA infusion. Our analyzes showed an immediate boost of glymphatic flow by PPA administration after KA (Fig. 6). Influx of CSF should reduce the accumulation of extracellular glutamate, K^+, and lactate, thereby facilitating the termination of seizure activity. In fact, PPA treatment alone increased the extracellular space volume[32], and accelerated the normalization of K^+ after spreading depression waves, thus resulting in faster restoration of normal EEG activity and evoked potentials[97]. The major electrophysiological effect of pan-adrenergic blockage after KA infusion was the shortening of the period of abnormal electrical activity and dampened epileptogenesis in the chronic phase (Fig. 1F). We speculate that boosting metabolic waste clearance accelerates the normalization of both glutamate, K^+, lactate, and lowers brain cytokine levels, thus facilitating the termination of seizure activity. We cannot exclude the possibility that inhibition of neuronal NE receptors also contributes to the shortening of the seizure. Yet, the complicated actions of NE in seizures discussed above suggest that non-neuronal mechanisms also are in play.

A limitation of this study is that the intracisternal magna infusion protocol we used (30 minutes circulation time and Bovine Serum Albumin/Ovalbumin fluorescent tracer, 66 kDa/45KDa) was not optimized for demonstrating hippocampal glymphatic influx. The influx of large CSF tracers into cortical regions are always higher than in the hippocampus[111–114]. Alternative approaches are needed to better assess glymphatic transport in the hippocampus, such as extending CM

infusion with longer circulation time (60 minutes) and using a smaller fluorescent tracer (Dextran, 6kD)[115] or in vivo MRI imaging with specific tracers[30].

Translational potentials and remaining uncertainties

Functional imaging has revealed that glymphatic activity is impaired in epileptic patients[21,116–120]. Due to the harmful consequences of epileptogenesis and recurrent seizures in epileptic patients, there is an urgent need to identify effective remediation strategies[7]. The antiepileptic drugs currently used in the clinic for acquired epilepsy include phenobarbital, phenytoin, carbamazepine and valproate[121]. Experimental studies have shown the effects of antioxidants, glutamatergic receptors, astrocytic glutamate uptake, anti-inflammatory substances, regulation of regeneration and neuroplasticity in the context of epileptogenesis[122]. Increasing brain "waste disposal" is a reasonable strategy for epileptic patients. The components of PPA, propranolol, prazosin, and atipamezole, are all clinically commonly used medications, but their possible side effects must necessarily be assessed. Fine-tuning of the combinations and proportions of the three antagonists might optimize the therapeutic effects, while minimizing side effects. The data presented here shows that glymphatic enhancement serves as an immediate responder during the initial SE as well as afterward and that potentiation of glymphatic flow, reduce the severity of the spontaneous seizures in the chronic epileptic phase.

Methods

Animals

FVB/2 J mice aged 8-12 weeks old and weighing 25–35 g were used for all experiments. AQP4 knockout mice aged 6 months old on a C57BL/6 background were the generous gift of Dr. Ming Xiao (Nanjing Medical University, China)[123]. Mice were housed in groups of five with a 12-hour light/dark cycle and *ad libitum* access to water and food in standard laboratory conditions. The committees on animal experimentation at the Universities of Rochester and Fudan separately approved all experiments (Protocol No. 2011-022 and 2011-023). The animal studies were performed in accordance with guidelines of the National Institutes of Health and Association for Assessment and Accreditation of Laboratory Animal Care (AAALAC) standards, and according to the Animal Experiment and Use Committee at the Shanghai Medical School of Fudan University (20200306-051). We randomly allocated mice to different experimental groups and made all efforts to minimize the animals' discomfort throughout the experiments.

Induction of status epilepticus

To induce status epilepticus (SE), mice were anesthetized at ZT 8 with 2 % isoflurane and fixed in a stereotaxic frame for drilling a 0.8 mm diameter cranial burr hole (Tech2000, RAM) over the right dorsal hippocampus. Directing a Hamilton syringe (65457-01, 0.5 µl, 32 gauge) at the coordinates AP = −1.8, ML = −1.6, and DV = 1.8 mm, we infused a 50 nl volume of 20 mM KA (Cat. K0250, Sigma-Aldrich, St. Louis, MO.) dissolved in saline. The infusion was performed at a rate of 10 nl/min, with the needle remaining in place for seven minutes prior to its withdrawal. To enable recording the electroencephalogram (EEG) and electromyogram (EMG) signals during SE, four-screw electrodes configured as in Fig. S1A were implanted on the frontal and somatosensory cortices of the hemisphere contralateral to infusion site, as previously reported[44,124], with placement of EMG wire-leads underneath the neck muscles. A group of mice received EEG/EMG electrodes together with an intrahippocampal cannula (PlasticsOne, Roanoke, VA) one-week prior to the KA infusion. In that setting, a 1 µl volume of 1 mM KA or saline vehicle was infused without anesthesia over five-minute period. Following surgery and for the next two days, mice were administered 1 ml i.p. 0.9% saline to prevent dehydration.

Treatment with pan-adrenergic inhibitor cocktail

After the intrahippocampal infusion of KA (post KA), mice received an i.p. injection of saline or a cocktail of noradrenergic receptor inhibitors/antagonists (PPA). For the PPA treatment, we followed a modification of the protocol in our prior studies[34,35,125]: The PPA mixture contained prazosin hydrochloride (6 mg/kg; Sigma Aldrich, Cat. P7791), propranolol hydrochloride (6 mg/kg; Tocris Bioscience, Cat. 0624), and atipamezole hydrochloride (0.6 mg/kg, Tocris Bioscience, Cat. 2937), prepared in 0.1% DMSO solution in 0.88 mL saline. According to the particular experiment, we administered PPA at five minutes (KA 5 min), 30 h (KA 30 hours), or three weeks (KA 3 weeks) post KA infusion. For KA 5 min and KA 30 hours mice, we gave three daily successive PPA doses at the same ZT time. For the KA 3 weeks mice, we gave a single PPA dose. Mice in the control groups received sham surgeries and one or three i.p. injections of vehicle (0.1 mL 0.1% DMSO in saline).

Behavioral evaluation of seizures

After intrahippocampal vehicle or KA infusion, mice were transferred to a recording chamber with 12-12 hr light cycle for 72 h of continuous infrared video recording (Samsung SDC-9443BC) and electrophysiological monitoring (details below) throughout the SE. The mice could move freely and had free access to food and water. Based on viewing of the video-recording, we ranked the convulsive behavior according to the modified 7-point Racine scale[126]: (0) Normal behaving; (1) immobility, motionless staring or sudden behavioral arrest; (2) head nodding, stiff tail or facial jerking; (3) isolated myoclonic jerks, neck jerks or cycling; (4) forelimb clonic seizure; (5) tonic–clonic seizure lying on belly or side; (6) convulsion with jumping or rear and falling; (7) convulsion culminating in death. The final score was the mean rating from two independent researchers.

The correspondence between behavioral and electrophysiological evaluation seizures

EEG/EMG Signals were collected with 8206-HR (Pinnacle Technology, KS) or Axon DigiData 1322a and Clampex 10.2 software with a sampling rate of 1 KHz. Referring to prior studies[127,128], a seizure with Racine scale of 4 or above corresponded to the following electrophysiological features in the EEG signals: (1) synchronized high-frequency firing of amplitude at least twice the baseline signal amplitude; (2) seizure lasting longer than 20 s; (3) seizure followed by post-ictal depression with flattened EEG amplitude[129]. Meanwhile, we measured tonic/clonic muscular contractions by the EMG electrodes. Seizures qualified as **convulsive seizures** from the EEG/EMG recordings, or by behavioral scoring of Racine scale ≥ 4. Seizures failing to meet the above criteria in EEG/EMG signals, or seizures with Racine scale <4 were categorized as **non-convulsive seizures**[130].

Electrophysiological assessment of the kainite-induced status epilepticus

During the first 30 hours after intrahippocampal KA infusion, a period of recurrent epileptic activity characterized by electrophysiological and behavioral features was defined as "established status epilepticus (SE)", due to its similarity with the phenotype occurring during SE in humans[131]. The "established SE" starts with the first convulsive seizure post KA infusion, and consists of two successive phases: In phase 1, animals exhibited predominantly recurrent convulsive (Racine scale ≥ 4) along with sparse non-convulsive seizures (Racine scale <4). Phase 1 ended if no more seizure onset in two hours after the last recorded convulsive seizure. Phase 1 was followed by phase 2, which was characterized by continuous spike-waves in the EEG signals, along with non-convulsive SE to behavioral assessment (Racine Scale <4). In phase 2, convulsive seizures could occur sparsely at intervals exceeding one hour. After the KA infusion, the spike-wave frequency first increased to a peak and then declined; we defined the end of phase 2 as the time

when spike-wave frequency had decreased to 0.1 Hz. The definition of phases is illustrated in Fig. 1 and Fig. S1.

Electrophysiological assessment of spontaneous epileptic discharges in chronic phase after SE

To evaluate the severity of the spontaneous epileptic discharges, we obtained video and EEG/EMG recording for four consecutive days at either three weeks or two months post KA. We defined the start of a spontaneous seizure as the time point when the EEG signal amplitude reached twice the baseline levels. The scoring of the spontaneous seizures was as described above **(Behavioral evaluation of seizures)**. Spontaneous interictal spikes prevalent in chronic phase were identified as isolated events of duration less than 100 ms with amplitude exceeding twice the baseline. The interictal spike frequency was automatically detected with a modification of a customized MATLAB script[132], and then manually checked. In brief, raw EEG signals were decomposed using wavelet analysis[133], and peaks of the interictal spikes were detected by the criterion of amplitude exceeding at least six fold the standard deviation of the decomposed signals during a one-hour epoch. Multiple peaks detected at intervals less than 1 s were counted as a single spike. Manual confirmation of automatically selected spikes indicated an error rate of 12.3%.

EEG power spectrum analysis

The EEG power spectrum was analyzed using a customized MATLAB script. The Chronux toolbox (http://chronux.org/) was used for the fast Fourier transform (FFT) and short-time Fourier transform (STFT), to plot the spectrogram, and to calculate the relative power for each of the four bands (delta, 0.5 to 4 Hz; theta, 4 to 8 Hz; alpha, 8 to 13 Hz; and beta, 13 to 32 Hz). We selected a five-second time window for STFT, and averaged the total power for each band for further analysis. We used FFT to calculate the power spectrum during a two-hour period of EEG recording, for comparing the EEG profile before and after PPA treatment.

Assessment of Glymphatic flow influx

We assessed glymphatic flow influx in awake mice as reported previously[134] at three time points after the initial intrahippocampal infusion of KA: (1) the early stage of SE at five hours post KA; (2) after the "established SE" at 30 h post KA; (3) in the chronic phase after three weeks post KA, and at the same time points in the control groups. In addition, we assessed glymphatic influx at 30 min after i.p. PPA or saline injection in *wildtype* (WT) mice. The glymphatic influx tracers Alexa Fluor 647 conjugated bovine serum albumin (BSA-647, 66 kDa) or alternatively Alexa Fluor 555 conjugated ovalbumin (OB-555, 45 kDa) (Invitrogen, Life Technologies, Eugene, OR, USA), were dissolved in artificial CSF to a concentration of 1% w/v for cisterna magna (CM) infusion. Prior studies have shown that the two tracers give comparable results[28,135]. A CM cannula was implanted one day prior to the infusion. The 10 µL total volume of tracer was infused into the CM with a Harvard Instruments syringe pump (Series 11 Elite) at an infusion rate of 1 µl/min for 10 min. After a 30-minute interval for circulation, the mice were rapidly anesthetized with 2.5% isoflurane and decapitated. Brains were carefully extracted and fixed by immersion in 4% paraformaldehyde (PFA) in phosphate-buffered saline solution (PBS) overnight at 4 °C, and cut the next day into 100 µm-thick coronal sections using a VTS1000 vibratome (Leica).

Coronal brain sections (rostral to caudal: −1.2, −0.8, −0.4, +0.2, +0.6 and +1.0 mm from bregma) were then imaged using a 0.63X lens with 2X magnification on an MVX10 microscope (Olympus) equipped with a Lumencore 1600 (Prior) light source, using the Metamorph Basic (Olympus) software. The tracer distribution was quantified by ImageJ software version 1.47 (National Institutes of Health, imagej.nih.gov/ij/). The area fraction of tracer distribution in the slice was determined using threshold criteria common to each set of experiments. To display the overall influx levels for each group, we averaged tracer distribution among the individuals within each group and normalized to an anatomic template for each rostral-to-caudal level. We obtained the alignments to the template by applying symmetric image normalization (SyN) for nonlinear registration with Advanced Normalization Tools (ANTs) 2.1.0 scripted with Python 3.7. The brain regional quantification of glymphatic influx was calculated in regions of interest (ROIs) for hippocampus, hypothalamus, dorsal cortex, and ventral cortex at the AP −1.2 mm level.

Assessment of the efficacy of substance clearance

We measured substance clearance according to published procedures[35,45]. In brief, mice were implanted with a guide cannula (26 G, C315G SPC, 4.5 mm below pedestal) sealed with a dummy cannula (33 G, C315DC/SP, 4.5 mm projection) (PlasticsOne, Roanoke, VA) into the right striatum (Bregma: AP + 0.6; ML −2.0, DV −3.3 mm). After 24 h, the mice were anesthetized (1.5% isoflurane) for surgical exposure of the left femoral vein for real-time imaging with a fluorescent stereo microscope (microscope: MVX10, Olympus; light: PRIOR Lumen 1600-LED; camera: Flash 4.0 digital, Hamamatsu). The dummy cannula was replaced with the inner cannula (33 G, C3151/SP, 0.1 mm projection). We then infused a total volume of 1 µl 4% w/v Direct Blue 53 (DB53, also known as Evans Blue, E2129, Sigma−Aldrich, US) dissolved in aCSF at a rate of 0.2 µl/min into the right striatum, in parallel with initiation of the imaging of the left femoral vein lumen at 488 nm. The imaging was recorded at 15 minutes intervals for up to two hours, during which time we maintained hydration of the exposed femoral tissue with 0.9% saline. The fluorescence images were converted to 8-bit format, and the mean pixel intensity in a circular ROI (Diameter = 0.1 mm) was calculated in ImageJ (NIH, USA). The ROI placement was confirmed by an overlaid autofluorescence image at 488 nm. An ROI of identical dimensions positioned at least 1 mm away from the femoral vein served for background correction.

Microdialysis and interstitial cytokine measurement

At three weeks after the initial treatment, the KA- or vehicle-treated mice were implanted with a guide cannula in the CA3 region of the right hippocampus (AP −2.5, ML + 3.0, DV −2.0 mm). After a three-day recovery from surgery, a microdialysis probe with 100 kDa cut-off (CMA 8 High Cut-Off PES: 100 kDa, Harvard Apparatus) was placed in the cannula. The probes were equilibrated by infusing artificial CSF (3.5 mM KCl, 119 mM NaCl, 1 mM $CaCl_2$, 0.8 mM $MgCl_2$, 10 mM HEPES) containing 5% BSA for one hour prior to sample collection. Dialysis samples of 30 µl volume were collected at a perfusion rate of 0.5 µl/min. The collected samples were immediately stored at −80 °C for later analysis of cytokine concentrations using the Mouse Cytokine Array / Chemokine Array 31-Plex (MD31, Eve Technologies Corporation, Calgary, Canada).

Blood–brain barrier permeability assay

Blood–brain barrier (BBB) permeability was measured following a published protocol[136]. Intrahippocampal cannula was implanted under 2% isoflurane anesthesia. As a positive control, some mice received lipopolysaccharide (LPS, 1 mg/ml, 10 mg/kg i.p., Cat# L2630, Sigma-Aldrich, St. Louis, MO) to induce BBB leakage, whereas the main experimental groups received an i.p. injection of with the same volume amount of saline. Mice received an intrahippocampal 1 µl infusion of 1 mM KA to induce SE, whereas control mice received 1 µl of saline vehicle. A subgroup of KA mice received i.p. PPA as described above. Twenty-four hours later, we infused 6 mg/kg cadaverine-594 (Invitrogen, Life Technologies, Eugene, OR, USA) at a volume of 14 ml/kg (0.43 mg/ml working solution in saline) into a femoral vein and allowed 30 min for circulation. The mice were then exsanguinated and perfused with PBS through the apex of the heart, prior to harvesting brain samples for placement in pre-weighed 5 ml tubes containing 500 µl

PBS. The tubes were re-weighed and the brains were homogenized, mixed with 1 M acetic acid, and incubated on ice for 10 min. After centrifugation at 10,000 x g for 10 min at 4 °C, the supernatant was carefully transferred for fluorescence measurement at an excitation wavelength of 590 nm and emission wavelength of 617 nm (SpectraMax Plus 384, Molecular Devices, USA). Fluorescence values were normalized to tissue weight.

Behavioral tests

For the open field test, we placed individual mice in an empty plastic box (30 × 50 cm) and video-recorded their exploration during a ten minute session. The total distance traveled during that period was traced and extracted by AnyMaze Software (Muromachi Kikai Co., Ltd. Japan). For the Rota-rod test, mice were placed on a Rota-Rod (Ugo Basile), which was set to accelerate from 5–40 rpm over a 5-minute session. We calculated the mean time to fall recorded in three testing sessions for each mouse, with a 30-minute rest period between each repetition. We repeated the test daily for three days to measure motor learning ability.

Immunohistochemistry

Mouse brains were perfusion-fixed with 4.0% paraformaldehyde (PFA). Following overnight post-fixation at 4 °C, coronal slices (100-µm thick) were prepared using a vibratome (VTS1000, Leica). Slices were permeabilized with 0.1% Triton-X-100 in PBS, blocked with 7% normal donkey serum (Jackson Immunoresearch) in PBS with 0.03% Triton-X-100, and then incubated with primary antibody overnight, followed by three washes in PBS and incubation with the fluorophore-linked secondary antibodies (Jackson Immunoresearch) for two hours. Stained slices were mounted with Fluoromount G (Thermofischer Scientific). Primary antibodies used were mouse anti-GFAP (1:500; Chemicon, MAB360), mouse anti-NeuN (1:500; Chemicon, MAB377), rat anti-CD68 (1:500; Serotec, MCA1957), and rabbit anti-AQP4 (1:500; Chemicon, AB3594), whereas cell nuclei were identified using DAPI staining (Invitrogen). Antibody dilutions were as follows: Cy2 donkey anti-rabbit (1:500; ThermoFisher Scientific), Cy2 donkey anti-mouse (1:500; ThermoFisher Scientific), Cy3 donkey anti-mouse (1:500; ThermoFisher Scientific), and Cy3 donkey anti-rat (1:500; ThermoFisher Scientific).

Imaging quantification

Immunostainings were imaged on a confocal microscope (IX81, Olympus) with and 40×/1.3 objective lens. For GFAP- and CD68-positive area analysis, we set fixed fluorescence intensities as thresholds for all images. The positive area ratio was the percentage of brain pixels exceeding that threshold. For NeuN-positive cell counting, all oval-shaped cells were counted within 0.5 × 0.5 µm ROIs. For quantification of AQP4 polarization, we followed a published previously method[137–140], as illustrated in Fig. S3B. In brief, representative 70 µm segments centered about vessels were analyzed using the line-plot tool in ImageJ. We classified vessels into two groups based on their diameter (small vessels <10 µm, large vessels 10–30 µm), and calculated the line polarization index (LPI) as the peak intensity of the vascular end-feet divided by the average of the baseline. We undertook this analysis with images at 20X magnification.

Statistical analysis

All data are presented as mean ± SEM. For each statistical comparison, normality was assessed with the Lilliefors test, and either parametric or non-parametric tests were chosen accordingly. For comparing more than one group, variance homogeneity was tested by Brown–Forsythe test or Bartlett's test, and multiple comparisons were made with one-way ANOVA and Tukey's multiple comparisons, or accordingly by Kruskal-Wallis and Dunn's multiple comparisons tests. All statistics were performed with the software Prism (GraphPad). The statistical method for each dataset is presented in the corresponding figure legend. A p-value of <0.05 was considered significant for rejecting the null hypothesis.

Reporting summary

Further information on research design is available in the Nature Portfolio Reporting Summary linked to this article.

Data availability

The data supporting the findings of this study are included in the figures and supporting files. Source data are provided with this paper. Minimum dataset was deposited to Zenodo (https://zenodo.org/records/13739055. https://doi.org/10.5281/zenodo.13739055). Source data are provided with this paper.

Code availability

Codes were deposited to Zenodo (https://zenodo.org/records/13739055. https://doi.org/10.5281/zenodo.13739055).

References

1. Fisher, R. S. et al. ILAE official report: a practical clinical definition of epilepsy. *Epilepsia* **55**, 475–482 (2014).
2. Blumenfeld, H. New strategies for preventing epileptogenesis: perspective and overview. *Neurosci. Lett.* **497**, 153–154 (2011).
3. Piccenna, L., Shears, G. & O'Brien, T. J. Management of post-traumatic epilepsy: an evidence review over the last 5 years and future directions. *Epilepsia Open* **2**, 123–144 (2017).
4. Roberg, L. E. et al. Prediction of long-term survival after status epilepticus using the ACD score. *JAMA Neurol.* **79**, 604–613 (2022).
5. Rogawski, M. A., Löscher, W. & Rho, J. M. Mechanisms of action of antiseizure drugs and the ketogenic diet. *Cold Spring Harb. Perspect. Med.* **6**, a022780 (2016).
6. Schmidt, D., Friedman, D. & Dichter, M. A. Anti-epileptogenic clinical trial designs in epilepsy: issues and options. *Neurotherapeutics* **11**, 401–411 (2014).
7. Binder, D. K. et al. Epilepsy benchmarks area II: prevent epilepsy and its progression. *Epilepsy Curr.* **20**, 14S–22S (2020).
8. Klein, P. & Tyrlikova, I. Prevention of epilepsy: should we be avoiding clinical trials? *Epilepsy Behav.* **72**, 188–194 (2017).
9. Amakhin, D. V. et al. Seizure-induced potentiation of AMPA receptor-mediated synaptic transmission in the entorhinal cortex. *Front. Cell. Neurosci.* **12**, 486 (2018).
10. Tyler, A. L. et al. Functional network changes in hippocampal CA1 after status epilepticus predict spatial memory deficits in rats. *J. Neurosci.* **32**, 11365–11376 (2012).
11. Butler, C. R., Westbrook, G. L. & Schnell, E. Adaptive mossy cell circuit plasticity after status epilepticus. *J. Neurosci.* **42**, 3025–3036 (2022).
12. Pun, R. Y. K. et al. Excessive activation of mTOR in postnatally-generated granule cells is sufficient to cause epilepsy. *Neuron* **75**, 1022–1034 (2012).
13. Chen, K., Baram, T. Z. & Soltesz, I. Febrile seizures in the developing brain result in persistent modification of neuronal excitability in limbic circuits. *Nat. Med.* **5**, 888–894 (1999).
14. Leite, J. P. et al. Plasticity, synaptic strength, and epilepsy: what can we learn from ultrastructural data? *Epilepsia* **46**, 134–141 (2005).
15. Ankarcrona, M. et al. Glutamate-induced neuronal death: a succession of necrosis or apoptosis depending on mitochondrial function. *Neuron* **15**, 961–973 (1995).
16. De Simoni, M. G. et al. Inflammatory cytokines and related genes are induced in the rat hippocampus by limbic status epilepticus. *Eur. J. Neurosci.* **12**, 2623–2633 (2000).
17. Debanne, D., Thompson, S. M. & Gähwiler, B. H. A brief period of epileptiform activity strengthens excitatory synapses in the rat hippocampus in vitro. *Epilepsia* **47**, 247–256 (2006).

18. Devinsky, O., Vezzani, A., Najjar, S., De Lanerolle, N. C. & Rogawski, M. A. Glia and epilepsy: excitability and inflammation. *Trends Neurosci.* **36**, 174–184 (2013).
19. Ergina, J. L., Amakhin, D. V., Postnikova, T. Y., Soboleva, E. B. & Zaitsev, A. V. Short-term epileptiform activity potentiates excitatory synapses but does not affect intrinsic membrane properties of pyramidal neurons in the rat hippocampus in vitro. *Biomedicines* **9**, 1374 (2021).
20. Fröhlich, F., Timofeev, I., Sejnowski, T. J. & Bazhenov, M. 26 - Extracellular Potassium Dynamics and Epileptogenesis. In *Computational Neuroscience in Epilepsy* (eds Soltesz, I. & Staley, K.) 419–439 (Academic Press, San Diego, 2008). https://doi.org/10.1016/B978-012373649-9.50029-6.
21. Liu, K. et al. Attenuation of cerebral edema facilitates recovery of glymphatic system function after status epilepticus. *JCI Insight* **6**, e151835 (2021).
22. Moody, W. J., Futamachi, K. J. & Prince, D. A. Extracellular potassium activity during epileptogenesis. *Exp. Neurol.* **42**, 248–263 (1974).
23. Sano, F. et al. Reactive astrocyte-driven epileptogenesis is induced by microglia initially activated following status epilepticus. *bioRxiv* 806398 (2019) https://doi.org/10.1101/806398.
24. Vezzani, A., Friedman, A. & Dingledine, R. J. The role of inflammation in epileptogenesis. *Neuropharmacology* **69**, 16–24 (2013).
25. Yaari, Y., Konnerth, A. & Heinemann, U. Nonsynaptic epileptogenesis in the mammalian hippocampus in vitro. II. Role of extracellular potassium. *J. Neurophysiol.* **56**, 424–438 (1986).
26. Hablitz, L. M. & Nedergaard, M. The glymphatic system: a novel component of fundamental neurobiology. *J. Neurosci.* **41**, 7698–7711 (2021).
27. Rasmussen, M. K., Mestre, H. & Nedergaard, M. Fluid transport in the brain. *Physiol. Rev.* https://doi.org/10.1152/physrev.00031.2020 (2021).
28. Iliff, J. J. et al. A paravascular pathway facilitates CSF flow through the brain parenchyma and the clearance of interstitial solutes, including amyloid β. *Sci. Transl. Med.* **4**, 147ra111–147ra111 (2012).
29. Harrison, I. F. et al. Impaired glymphatic function and clearance of tau in an Alzheimer's disease model. *Brain* **143**, 2576–2593 (2020).
30. Mestre, H. et al. Aquaporin-4-dependent glymphatic solute transport in the rodent brain. *eLife* **7**, e40070 (2018).
31. Hablitz, L. M. et al. Circadian control of brain glymphatic and lymphatic fluid flow. *Nat. Commun.* **11**, 4411 (2020).
32. Xie, L. et al. Sleep drives metabolite clearance from the adult brain. *Science* **342**, 373–377 (2013).
33. He, X.-F. et al. Overexpression of Slit2 decreases neuronal excitotoxicity, accelerates glymphatic clearance, and improves cognition in a multiple microinfarcts model. *Mol. Brain* **13**, 135 (2020).
34. Monai, H. et al. Adrenergic receptor antagonism induces neuroprotection and facilitates recovery from acute ischemic stroke. *Proc. Natl Acad. Sci.* **116**, 11010–11019 (2019).
35. Hussain, R. et al. Potentiating glymphatic drainage minimizes post-traumatic cerebral oedema. *Nature* https://doi.org/10.1038/s41586-023-06737-7 (2023).
36. Lévesque, M. & Avoli, M. The kainic acid model of temporal lobe epilepsy. *Neurosci. Biobehav. Rev.* **37**, 2887–2899 (2013).
37. Rusina, E., Bernard, C. & Williamson, A. The kainic acid models of temporal lobe epilepsy. *eNeuro* **8**, ENEURO.0337-20.2021 (2021).
38. Sharma, A. K. et al. Mesial temporal lobe epilepsy: pathogenesis, induced rodent models and lesions. *Toxicol. Pathol.* **35**, 984–999 (2007).
39. Téllez-Zenteno, J. F. & Hernández-Ronquillo, L. A review of the epidemiology of temporal lobe epilepsy. *Epilepsy Res. Treat.* **2012**, 630853 (2012).
40. Margerison, J. H. & Corsellis, J. A. Epilepsy and the temporal lobes. A clinical, electroencephalographic and neuropathological study of the brain in epilepsy, with particular reference to the temporal lobes. *Brain J. Neurol.* **89**, 499–530 (1966).
41. Nayak, C. S. & Bandyopadhyay, S. Mesial Temporal Lobe Epilepsy. in *StatPearls* (StatPearls Publishing, Treasure Island (FL), 2022).
42. Kandratavicius, L. et al. Animal models of epilepsy: use and limitations. *Neuropsychiatr. Dis. Treat.* **10**, 1693–1705 (2014).
43. Lisgaras, C. P. & Scharfman, H. E. Robust chronic convulsive seizures, high frequency oscillations, and human seizure onset patterns in an intrahippocampal kainic acid model in mice. *Neurobiol. Dis.* **166**, 105637 (2022).
44. Hablitz, L. M. et al. Increased glymphatic influx is correlated with high EEG delta power and low heart rate in mice under anesthesia. *Sci. Adv.* **5**, eaav5447 (2019).
45. Plá, V. et al. A real-time in vivo clearance assay for quantification of glymphatic efflux. *Cell Rep.* **40**, 111320 (2022).
46. Rash, J. E., Yasumura, T., Hudson, C. S., Agre, P. & Nielsen, S. Direct immunogold labeling of aquaporin-4 in square arrays of astrocyte and ependymocyte plasma membranes in rat brain and spinal cord. *Proc. Natl Acad. Sci. Usa.* **95**, 11981–11986 (1998).
47. Nielsen, S. et al. Specialized membrane domains for water transport in glial cells: high-resolution immunogold cytochemistry of aquaporin-4 in rat brain. *J. Neurosci. J. Soc. Neurosci.* **17**, 171–180 (1997).
48. Mohajeri, M. H. et al. The impact of genetic background on neurodegeneration and behavior in seizured mice. *Genes Brain Behav.* **3**, 228–239 (2004).
49. Schauwecker, P. E. & Steward, O. Genetic determinants of susceptibility to excitotoxic cell death: implications for gene targeting approaches. *Proc. Natl Acad. Sci. Usa.* **94**, 4103–4108 (1997).
50. Dulla, C. G. & Pitkänen, A. Novel approaches to prevent epileptogenesis after traumatic brain injury. *Neurotherapeutics* **18**, 1582–1601 (2021).
51. Fordington, S. & Manford, M. A review of seizures and epilepsy following traumatic brain injury. *J. Neurol.* **267**, 3105–3111 (2020).
52. Izadi, A. et al. Early intervention via stimulation of the medial septal nucleus improves cognition and alters markers of epileptogenesis in pilocarpine-induced epilepsy. *Front. Neurol.* **12**, 708957 (2021).
53. Liou, J.-H. et al. Preventing epilepsy after traumatic brain injury: a propensity score analysis. *J. Chin. Med. Assoc.* **83**, 950–955 (2020).
54. Dunwiddie, T. V., Taylor, M., Heginbotham, L. R. & Proctor, W. R. Long-term increases in excitability in the CA1 region of rat hippocampus induced by beta-adrenergic stimulation: possible mediation by cAMP. *J. Neurosci.* **12**, 506–517 (1992).
55. Fink, A. E. & LeDoux, J. E. β-Adrenergic enhancement of neuronal excitability in the lateral amygdala is developmentally gated. *J. Neurophysiol.* **119**, 1658–1664 (2018).
56. Scanziani, M., Gahwiler, B. H. & Thompson, S. M. Presynaptic inhibition of excitatory synaptic transmission mediated by alpha adrenergic receptors in area CA3 of the rat hippocampus in vitro. *J. Neurosci.* **13**, 5393–5401 (1993).
57. Bellesi, M., Tononi, G., Cirelli, C. & Serra, P. A. Region-specific dissociation between cortical noradrenaline levels and the sleep/wake cycle. *Sleep* **39**, 143–154 (2016).
58. Hanlon, E. C., Vyazovskiy, V. V., Faraguna, U., Tononi, G. & Cirelli, C. Synaptic potentiation and sleep need: clues from molecular and electrophysiological studies. *Curr. Top. Med. Chem.* **11**, 2472–2482 (2011).
59. El-Etri, M. M., Ennis, M., Jiang, M. & Shipley, M. T. Pilocarpine-induced convulsions in rats: evidence for muscarinic receptor-mediated activation of locus coeruleus and norepinephrine release in cholinolytic seizure development. *Exp. Neurol.* **121**, 24–39 (1993).
60. Fitzgerald, P. J. Is elevated norepinephrine an etiological factor in some cases of epilepsy? *Seizure* **19**, 311–318 (2010).

61. Svob Strac, D. et al. Monoaminergic mechanisms in epilepsy may offer innovative therapeutic opportunity for monoaminergic multitarget drugs. *Front. Neurosci.* **10**, 492 (2016).
62. De Fusco, M. et al. The α2B adrenergic receptor is mutant in cortical myoclonus and epilepsy. *Ann. Neurol.* **75**, 77–87 (2014).
63. Ahmadirad, N. et al. The role of α adrenergic receptors in mediating the inhibitory effect of electrical brain stimulation on epileptiform activity in rat hippocampal slices. *Brain Res* **1765**, 147492 (2021).
64. Biagioni, F. et al. Noradrenaline and seizures: a perspective on the role of adrenergic receptors in limbic seizures. *Curr. Neuropharmacol.* **20**, 1–4 (2022).
65. Hazra, A. et al. β-Adrenergic modulation of spontaneous spatiotemporal activity patterns and synchrony in hyperexcitable hippocampal circuits. *J. Neurophysiol.* **108**, 658–671 (2012).
66. Biggane, J. P. et al. Pharmacological characterization of the α2A-adrenergic receptor inhibiting rat hippocampal CA3 epileptiform activity: comparison of ligand efficacy and potency. *J. Recept. Signal Transduct.* **0**, 1–8 (2022).
67. de Curtis, M. & Avanzini, G. Interictal spikes in focal epileptogenesis. *Prog. Neurobiol.* **63**, 541–567 (2001).
68. Lillis, K. P. et al. Evolution of network synchronization during early epileptogenesis parallels synaptic circuit alterations. *J. Neurosci.* **35**, 9920–9934 (2015).
69. Morimoto, K., Fahnestock, M. & Racine, R. J. Kindling and status epilepticus models of epilepsy: rewiring the brain. *Prog. Neurobiol.* **73**, 1–60 (2004).
70. Staley, K. J. & Dudek, F. E. Interictal spikes and epileptogenesis. *Epilepsy Curr.* **6**, 199–202 (2006).
71. Lundgaard, I. et al. Glymphatic clearance controls state-dependent changes in brain lactate concentration. *J. Cereb. Blood Flow. Metab. J. Int. Soc. Cereb. Blood Flow. Metab.* **37**, 2112–2124 (2017).
72. Hesdorffer, D. C., Logroscino, G., Cascino, G., Annegers, J. F. & Hauser, W. A. Risk of unprovoked seizure after acute symptomatic seizure: Effect of status epilepticus. *Ann. Neurol.* **44**, 908–912 (1998).
73. French, J. A. et al. Characteristics of medial temporal lobe epilepsy: I. results of history and physical examination. *Ann. Neurol.* **34**, 774–780 (1993).
74. Mathern, G. W., Pretorius, J. K. & Babb, T. L. Influence of the type of initial precipitating injury and at what age it occurs on course and outcome in patients with temporal lobe seizures. *J. Neurosurg.* **82**, 220–227 (1995).
75. Arkhipov, V., Kulesskaja, N. & Lebedev, D. Behavioral perseveration and impairment of long-term memory in rats after intrahippocampal injection of kainic acid in subconvulsive dose. *Pharmacol. Biochem. Behav.* **88**, 299–305 (2008).
76. Bragin, A., Azizyan, A., Almajano, J., Wilson, C. L. & Engel, J. Analysis of chronic seizure onsets after intrahippocampal kainic acid injection in freely moving rats. *Epilepsia* **46**, 1592–1598 (2005).
77. Cavalheiro, E. A., Riche, D. A. & Le Gal La Salle, G. Long-term effects of intrahippocampal kainic acid injection in rats: a method for inducing spontaneous recurrent seizures. *Electroencephalogr. Clin. Neurophysiol.* **53**, 581–589 (1982).
78. Klee, R., Brandt, C., Töllner, K. & Löscher, W. Various modifications of the intrahippocampal kainate model of mesial temporal lobe epilepsy in rats fail to resolve the marked rat-to-mouse differences in type and frequency of spontaneous seizures in this model. *Epilepsy Behav. EB* **68**, 129–140 (2017).
79. Rattka, M., Brandt, C. & Löscher, W. The intrahippocampal kainate model of temporal lobe epilepsy revisited: epileptogenesis, behavioral and cognitive alterations, pharmacological response, and hippoccampal damage in epileptic rats. *Epilepsy Res* **103**, 135–152 (2013).
80. Jensen, F. E., Applegate, C. D., Holtzman, D., Belin, T. R. & Burchfiel, J. L. Epileptogenic effect of hypoxia in the immature rodent brain. *Ann. Neurol.* **29**, 629–637 (1991).
81. Sanchez, R. M. Epileptogenesis After Ischemic-Hypoxic Encephalopathy. In *Atlas of Epilepsies* (ed. Panayiotopoulos, C. P.) 343–347 (Springer, London, 2010). https://doi.org/10.1007/978-1-84882-128-6_44.
82. Borowicz-Reutt, K. K. & Czuczwar, S. J. Role of oxidative stress in epileptogenesis and potential implications for therapy. *Pharmacol. Rep.* **72**, 1218–1226 (2020).
83. Martinc, B., Grabnar, I. & Vovk, T. The role of reactive species in epileptogenesis and influence of antiepileptic drug therapy on oxidative stress. *Curr. Neuropharmacol.* **10**, 328–343 (2012).
84. Ambrogini, P. et al. Excitotoxicity, neuroinflammation and oxidant stress as molecular bases of epileptogenesis and epilepsy-derived neurodegeneration: The role of vitamin E. *Biochim. Biophys. Acta BBA - Mol. Basis Dis.* **1865**, 1098–1112 (2019).
85. Frasca, A. et al. Misplaced NMDA receptors in epileptogenesis contribute to excitotoxicity. *Neurobiol. Dis.* **43**, 507–515 (2011).
86. Zorec, R. et al. Astroglial excitability and gliotransmission: an appraisal of Ca2+ as a signalling route. *ASN NEURO* **4**, e00080 (2012).
87. Chao, C. C. et al. Cytokine-stimulated astrocytes damage human neurons via a nitric oxide mechanism. *Glia* **16**, 276–284 (1996).
88. Rothwell, N. J. Cytokines – killers in the brain? *J. Physiol.* **514**, 3–17 (1999).
89. Marchi, N. et al. Seizure-promoting effect of blood–brain barrier disruption. *Epilepsia* **48**, 732–742 (2007).
90. van Vliet, E. A., Aronica, E. & Gorter, J. A. Blood–brain barrier dysfunction, seizures and epilepsy. *Semin. Cell Dev. Biol.* **38**, 26–34 (2015).
91. Cavazos, J. E. & Cross, D. J. The role of synaptic reorganization in mesial temporal lobe epilepsy. *Epilepsy Behav. EB* **8**, 483–493 (2006).
92. Cross, D. J. & Cavazos, J. E. Synaptic reorganization in subiculum and CA3 after early-life status epilepticus in the kainic acid rat model. *Epilepsy Res* **73**, 156–165 (2007).
93. Sutula, T., He, X.-X., Cavazos, J. & Scott, G. Synaptic reorganization in the hippocampus induced by abnormal functional activity. *Science* **239**, 1147–1150 (1988).
94. Scanzano, A. & Cosentino, M. Adrenergic regulation of innate immunity: a review. *Front. Pharmacol.* **6**, 171 (2015).
95. Gyoneva, S. & Traynelis, S. F. Norepinephrine Modulates The Motility Of Resting And Activated Microglia Via Different Adrenergic Receptors. *J. Biol. Chem.* **288**, 15291–15302 (2013).
96. Lechtenberg, K. J., Meyer, S. T., Doyle, J. B., Peterson, T. C. & Buckwalter, M. S. Augmented β2-adrenergic signaling dampens the neuroinflammatory response following ischemic stroke and increases stroke size. *J. Neuroinflammation* **16**, 112 (2019).
97. Monai, H. et al. Adrenergic receptor antagonism induces neuroprotection and facilitates recovery from acute ischemic stroke. *Proc. Natl Acad. Sci. Usa.* **116**, 11010–11019 (2019).
98. Ding, Y. et al. Astrogliosis inhibition attenuates hydrocephalus by increasing cerebrospinal fluid reabsorption through the glymphatic system after germinal matrix hemorrhage. *Exp. Neurol.* **320**, 113003 (2019).
99. Natário, K. H. P., Aguiar, G. B. & Vieira, M. A. D. C. E. S. The glymphatic system and its relation with neurological diseases. *Rev. Assoc. Médica Bras.* **67**, 620–624 (2021).
100. Meng, F. & Yao, L. The role of inflammation in epileptogenesis. *Acta Epileptol.* **2**, 15 (2020).
101. Fultz, N. E. et al. Coupled electrophysiological, hemodynamic, and cerebrospinal fluid oscillations in human sleep. *Science* **366**, 628–631 (2019).

102. Tønnesen, J., Inavalli, V. V. G. K. & Nägerl, U. V. Super-resolution imaging of the extracellular space in living brain tissue. *Cell* **172**, 1108–1121.e15 (2018).
103. Slais, K. et al. Brain metabolism and diffusion in the rat cerebral cortex during pilocarpine-induced status epilepticus. *Exp. Neurol.* **209**, 145–154 (2008).
104. Colbourn, R. et al. Rapid volume pulsation of the extracellular space coincides with epileptiform activity in mice and depends on the NBCe1 transporter. *J. Physiol.* **599**, 3195–3220 (2021).
105. Binder, D. K. et al. Increased seizure duration and slowed potassium kinetics in mice lacking aquaporin-4 water channels. *Glia* **53**, 631–636 (2006).
106. Szu, J. I., Patel, D. D., Chaturvedi, S., Lovelace, J. W. & Binder, D. K. Modulation of posttraumatic epileptogenesis in aquaporin-4 knockout mice. *Epilepsia* **61**, 1503–1514 (2020).
107. Lee, D. J. et al. Aquaporin-4-dependent edema clearance following status epilepticus. *Epilepsy Res* **98**, 264–268 (2012).
108. Verkman, A. S., Binder, D. K., Bloch, O., Auguste, K. & Papadopoulos, M. C. Three distinct roles of aquaporin-4 in brain function revealed by knockout mice. *Biochim Biophys. Acta* **1758**, 1085–1093 (2006).
109. Thrane, A. S. et al. Critical role of aquaporin-4 (AQP4) in astrocytic Ca2+ signaling events elicited by cerebral edema. *Proc. Natl Acad. Sci. Usa.* **108**, 846–851 (2011).
110. Verkman, A. S. Diffusion in the extracellular space in brain and tumors. *Phys. Biol.* **10**, 045003 (2013).
111. Spallazzi, M. et al. Hippocampal vascularization patterns: a high-resolution 7 Tesla time-of-flight magnetic resonance angiography study. *NeuroImage Clin.* **21**, 101609 (2019).
112. Erdem, A., Yaşargil, G. & Roth, P. Microsurgical anatomy of the hippocampal arteries. *J. Neurosurg.* **79**, 256–265 (1993).
113. Haegelen, C., Berton, E., Darnault, P. & Morandi, X. A revised classification of the temporal branches of the posterior cerebral artery. *Surg. Radiol. Anat. SRA* **34**, 385–391 (2012).
114. Johnson, A. C. Hippocampal vascular supply and its role in vascular cognitive impairment. *Stroke* **54**, 673–685 (2023).
115. Jiang-Xie, L.-F. et al. Neuronal dynamics direct cerebrospinal fluid perfusion and brain clearance. *Nature* **627**, 157–164 (2024).
116. Lee, D. A. et al. Glymphatic system function in patients with newly diagnosed focal epilepsy. *Brain Behav.* **12**, e2504 (2022).
117. Eid, T. et al. Loss of perivascular aquaporin 4 may underlie deficient water and K+ homeostasis in the human epileptogenic hippocampus. *Proc. Natl Acad. Sci. USA* **102**, 1193–1198 (2005).
118. Lee, D. A. et al. Glymphatic system dysfunction in temporal lobe epilepsy patients with hippocampal sclerosis. *Epilepsia Open* **7**, 306–314 (2022).
119. Lee, H.-J., Lee, D. A., Shin, K. J. & Park, K. M. Glymphatic system dysfunction in patients with juvenile myoclonic epilepsy. *J. Neurol.* https://doi.org/10.1007/s00415-021-10799-w (2021).
120. Pu, W. et al. Dysfunction of the glymphatic system in childhood absence epilepsy. *Front. Neurosci.* **17**, (2023).
121. National Institute for Health and Care Excellence. *Epilepsies in Children, Young People and Adults (NG217)*. 152 https://www.nice.org.uk/guidance/ng217 (2022).
122. Pitkänen, A., Lukasiuk, K., Dudek, F. E. & Staley, K. J. Epileptogenesis. *Cold Spring Harb. Perspect. Med.* **5**, a022822 (2015).
123. Fan, Y. et al. Sex- and region-specific alterations of basal amino acid and monoamine metabolism in the brain of aquaporin-4 knockout mice. *J. Neurosci. Res* **82**, 458–464 (2005).
124. Hauglund, N. L., Kusk, P., Kornum, B. R. & Nedergaard, M. Meningeal lymphangiogenesis and enhanced glymphatic activity in mice with chronically implanted EEG electrodes. *J. Neurosci.* https://doi.org/10.1523/JNEUROSCI.2223-19.2020 (2020).
125. Monai, H. et al. Adrenergic inhibition facilitates normalization of extracellular potassium after cortical spreading depolarization. *Sci. Rep.* **11**, 8150 (2021).
126. Racine, R. J. Modification of seizure activity by electrical stimulation. II. motor seizure. *Electroencephalogr. Clin. Neurophysiol.* **32**, 281–294 (1972).
127. Jagirdar, R., Drexel, M., Kirchmair, E., Tasan, R. O. & Sperk, G. Rapid changes in expression of class I and IV histone deacetylases during epileptogenesis in mouse models of temporal lobe epilepsy. *Exp. Neurol.* **273**, 92–104 (2015).
128. Puttachary, S. et al. Immediate epileptogenesis after kainate-induced status epilepticus in C57BL/6J mice: evidence from long term continuous video-EEG telemetry. *PLOS ONE* **10**, e0131705 (2015).
129. Bouilleret, V. et al. Recurrent seizures and hippocampal sclerosis following intrahippocampal kainate injection in adult mice: electroencephalography, histopathology and synaptic reorganization similar to mesial temporal lobe epilepsy. *Neuroscience* **89**, 717–729 (1999).
130. Smith, Z. Z., Benison, A. M., Bercum, F. M., Dudek, F. E. & Barth, D. S. Progression of convulsive and nonconvulsive seizures during epileptogenesis after pilocarpine-induced status epilepticus. *J. Neurophysiol.* **119**, 1818–1835 (2018).
131. Trinka, E. et al. A definition and classification of status epilepticus – report of the ILAE task force on classification of status epilepticus. *Epilepsia* **56**, 1515–1523 (2015).
132. Bergstrom, R. A. et al. Automated identification of multiple seizure-related and interictal epileptiform event types in the EEG of mice. *Sci. Rep.* **3**, 1483 (2013).
133. Adeli, H., Zhou, Z. & Dadmehr, N. Analysis of EEG records in an epileptic patient using wavelet transform. *J. Neurosci. Methods* **123**, 69–87 (2003).
134. Plog, B. A. et al. Transcranial optical imaging reveals a pathway for optimizing the delivery of immunotherapeutics to the brain. *JCI Insight* **3**, e120922 (2018).
135. Iliff, J. J. et al. Impairment of glymphatic pathway function promotes tau pathology after traumatic brain injury. *J. Neurosci.* **34**, 16180–16193 (2014).
136. Goldim, M. P., de, S., Della Giustina, A. & Petronilho, F. Using evans blue dye to determine blood-brain barrier integrity in rodents. *Curr. Protoc. Immunol.* **126**, e83 (2019).
137. Kress, B. T. et al. Impairment of paravascular clearance pathways in the aging brain. *Ann. Neurol.* **76**, 845–861 (2014).
138. Wang, M. et al. Cognitive deficits and delayed neuronal loss in a mouse model of multiple microinfarcts. *J. Neurosci.* **32**, 17948–17960 (2012).
139. Ren, Z. et al. 'Hit & Run' model of closed-skull traumatic brain injury (TBI) reveals complex patterns of post-traumatic AQP4 dysregulation. *J. Cereb. Blood Flow. Metab.* **33**, 834–845 (2013).
140. Lundgaard, I. et al. Beneficial effects of low alcohol exposure, but adverse effects of high alcohol intake on glymphatic function. *Sci. Rep.* **8**, 2246 (2018).

Acknowledgements

This work was supported by National Institutes of Health grant R01AT011439 (M.N.), National Institutes of Health grant U19NS128613 (M.N.), US Army Research Office grant MURI W911NF1910280 (M.N.), Human Frontier Science Program grant RGP0036 (M.N.), the Dr. Miriam and Sheldon G. Adelson Medical Research Foundation (M.N.), and Simons Foundation grant 811237 (M.N.). We thank Dr. Ming Xiao kindly provided the transgenic strain AQP4 Knockout mice. We would like to thank Yusi Hu, Divya Naidu and Brianna Roy for technical work, Prof. Paul Cumming of Bern University for comments on the manuscript, and Dan Xue for assistance with graphics.

Author contributions

Qian Sun, Sisi Peng, Pia Weikop, Rashad Hussain, Wei Song, and Qiwu Xu conducted the experiments; Qian Sun, Fengfei Ding analyzed the data and prepared the figures and manuscript. Maiken Nedergaard and Fengfei Ding designed the experiments.

Competing interests

The authors declare no competing interests.

Additional information

Supplementary information The online version contains supplementary material available at https://doi.org/10.1038/s41467-024-53430-y.

Correspondence and requests for materials should be addressed to Maiken Nedergaard or Fengfei Ding.

Peer review information *Nature Communications* thanks Davide Boido, Dipan Patel and the other anonymous reviewer(s) for their contribution to the peer review of this work. A peer review file is available.